Elongated self-assembled nanocarriers: From molecular organization to therapeutic applications

Julie Mougin, Claudie Bourgaux, Patrick Couvreur

Elongated self-assembled nanocarriers: from molecular organization to therapeutic applications

Author names and affiliations: Julie Mougin, Claudie Bourgaux, Patrick Couvreur

Institut Galien Paris-Saclay, UMR CNRS 8612, Faculty of Pharmacy, University Paris-Saclay, 92290 Châtenay-Malabry, France

Julie Mougin: julie.mougin@u-psud.fr

Claudie Bourgaux: claudie.bourgaux@u-psud.fr

Patrick Couvreur: patrick.couvreur@u-psud.fr (corresponding author)

UMR CNRS 8612
Institut Galien Paris-Saclay
Faculté de Pharmacie Paris-Sud
5 rue Jean-Baptiste Clément
92290 Châtenay-Malabry
France

Declarations of interest: P. Couvreur is the founder of the start-up company Squal Pharma.

Abstract

Self-assembled cylindrical aggregates made of amphiphilic molecules emerged almost 40 years ago. Due to their length up to micrometers, those particles display original physico-chemical properties such as important flexibility and, for concentrated samples, a high viscoelasticity making them suitable for a wide range of industrial applications. However, a quarter of century was needed to successfully take advantage of those improvements towards therapeutic purposes. Since then, a wide diversity of biocompatible materials such as polymers, lipids or peptides, have been developed to design self-assembling elongated drug nanocarriers, suitable for therapeutic or diagnostic applications. More recently, the investigation of the main forces driving the unidirectional growth of these nanodevices allowed a translation toward the formation of pure nanodrugs to avoid the use of unnecessary side materials and the possible toxicity concerns associated.

Keywords

Filomicelles, nanofibers, nanorods, drug delivery, polymers, lipids, peptides, bioconjugates, hydrogels, nanodrugs

1. Introduction

Drug nanocarriers represent a very active area of research, particularly in oncology, as they can increase drug efficacy by improving drug pharmacokinetics and biodistribution. Spherical nanocarriers, such as micelles, liposomes or polymer nanoparticles are generally used. The first biological barrier encountered by these nanocarriers after intravenous administration is their rapid clearance from the blood compartment by the phagocytic cells from the reticulo-endothelial system (RES), triggered by the adsorption of plasma proteins at their surface (the so-called "opsonization").[1,2] Nanoparticles size significantly influences the protein corona formation so that a longer circulation time is obtained with nanocarriers with a size of ~ 20 nm and below. Surface

modification with hydrophilic brushes of poly(ethylene glycol) (PEG) may further hinder opsonization, leading also to extended lifetime in the blood stream of these "stealth" PEGylated particles.[3,4] However, the shape of the nanocarriers also matters. Early *in vitro* studies by Mitragotri and colleagues have highlighted the role of the particle shape in phagocytosis.[5–7] They showed that whether rat alveolar macrophages initiated phagocytosis or spreading on anisotropic polystyrene (PS) particles depended on the local particle shape at the initial point of contact. A sharp geometry at the point of contact favored internalization. In contrast, phagocytosis did not occur when the long axis of a prolate ellipsoid was parallel to the cell membrane. Prolate ellipsoids were internalized much less efficiently than oblate ellipsoids or spheres and phagocytosis was inhibited for elongated particles with aspect ratios higher than 20.

The pioneering researches initiated by Discher's group revealed an unprecedented delayed clearance *in vivo* for long flexible micelles self-assembled from amphiphilic, PEG-based, diblock copolymers.[8] These so-called "filomicelles", reminiscent of filoviruses in some respects, persisted in the rodent blood stream up to one week for 8 µm-long ones, in spite of their progressive fragmentation. This is about ten times longer than for spherical particles with similar surface chemistry. The filomicelles were stretched by the flow and aligned along the stream lines, thereby reducing vessel wall collisions and interactions with macrophages **(Fig. 1)**. To assess the potential of these filomicelles as new drug delivery devices, they were loaded with paclitaxel (PTX), a hydrophobic drug active against a wide range of cancers.[9,10] The maximum tolerated dose (MTD) was almost two-fold higher for PTX in filomicelles than when loaded in spherical micelles resulting in a greater and more sustained tumor shrinkage in a mice xenografted model of lung cancer.

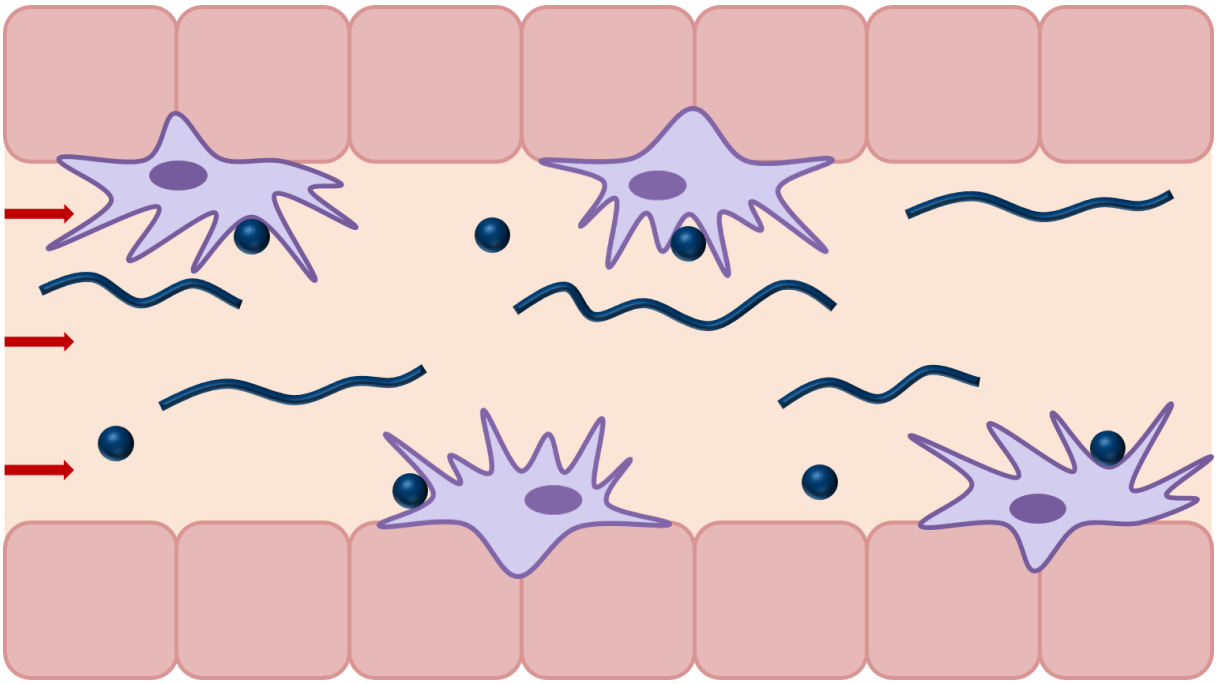

Fig. 1: Scheme of the different uptake of spherical and cylindrical micelles (dark blue) by macrophages (pale blue) under blood flow. The red arrows indicate the blood flow direction.

These outstanding results have stimulated interest in developing new cylindrical drug carriers and in investigating how the design parameters can affect the transport, biodistribution, targeting and cellular internalization of particles by non-phagocytic cells upon intravenous administration. Recent reports have attempted to define general guidelines for efficient drug carrier.[11–16] This is a complex task because controlled sizes and shapes combine with other parameters such as flexibility and surface properties to collectively determine the fate of the particles and because optimized parameters are not necessarily the same for each successive stage of the particle pathway *in vivo*. Beyond the influence of size and shape on phagocytosis, numerous simulation and experimental studies have investigated the impact of size and shape on migration (margination) and adhesion to the vessel walls, extravasation through pores, accumulation at the disease site and cellular internalization of the particles. New top-down fabrication methods have opened the possibility to compare particles with identical volumes but different shapes, including rods or worms.[17,18] Mitragotri's group have used a stretching process to deform spherical PS or poly(lactic-co-glycolic acid) (PLGA)-based particles embedded in a poly(vinyl alcohol) (PVA) film,

achieving particles with complex shapes.[5] The Particle Replication in Nonwetting Templates (PRINT) method, developed by DeSimone's group, enabled also precise control over the size and shape of molded particles usually composed of polylactic acid (PLA) or PEG hydrogels whose elastic modulus can be tuned by cross-linking. However, few reports have dealt with top-down-made particles loaded with a therapeutic substance and, to our knowledge, none has compared the therapeutic performances of cylindrical nanomedicines and spherical ones.[19,20]

Most often, the formation of cylindrical drug nanocarriers relies on the self-assembly in an aqueous medium of amphiphilic molecules (*e.g.* block copolymers, peptide amphiphiles, lipid- or polymer-based bioconjugates…), driven by the aggregation of the hydrophobic moieties. The morphology of these cylindrical assemblies is mainly controlled by the wedge shape of the molecules. It can also be tuned by a variation of temperature or pH, or by the concentration and nature of ions in solution when the hydrophilic part of the molecules displays pH-sensitive or charged groups.[21,22] For example, the phase diagram of the near-symmetric poly(acrylic acid)-polybutadiene (PAA-PBD) charged block copolymer showed that the self-assembly morphology switched from spherical micelles to cylinders and from cylinders to vesicles (with broad coexistence regions) when adding salt or decreasing the pH from pH = 8 to pH = 3. Within the cylindrical micelle region, decreasing further the repulsions between the PAA corona blocks by neutralizing or screening their charges entailed the growth of worm-like micelles up to several microns long.[22] This example illustrates the difficulty to generate different shapes based on a unique chemical composition in the same conditions. However, in some cases, spherical micelles could be kinetically stabilized by sonication or high-pressure homogenization of the worm-like micelles.

Finally, the effectiveness of nanocarriers depends on their drug loading capacity and their ability to deliver it to the site of action. The so-called "physical encapsulation" of drugs consists in the formulation of a nanocarrier in which the non-covalently bound drug is physically entrapped, either in the hydrophobic core or at the surface, depending on the drug properties. However, this approach may require a purification step to remove the non-encapsulated drug, and often leads to poor drug loading and possible burst release of the drug molecules when they are only adsorbed at the surface of the

nanocarrier. Considering spherical and cylindrical nanocarriers with equal radius, nanocylinders exhibit a higher volume-to-surface ratio. Hence, when the drug is entrapped in the nanocarrier core, the drug loading in cylindrical nanocarriers should be higher than in spherical ones. The drug release is also expected to depend on the nanocarrier shape, due to the dependence of diffusion/dissolution on geometry. The influence of drug-carrier interactions on drug loading and release has also been unveiled, weaker interactions inducing lower encapsulation efficiency and loading and faster release. The composition and the diameter of the filomicelles core could be tuned with the aim to achieve a high drug loading capacity and a sustained drug release.[23–25] The covalent coupling of the drug to the nanocarrier material to form amphiphilic bioconjugates able to self-assemble allowed overcoming some of the limitations of the physical encapsulation. Depending on the molecular weight of the carrier molecule, the so-called "chemical encapsulation" allows generally higher drug loading, while avoiding burst release. Additionally, the incorporation of stimuli-sensitive linkers between the drug and the carrier material enables precise control of the drug release. However, both physical and chemical loading involve the use of a carrier material which can have safety concern. Therefore, recent trends have focused on the development of carrier-free pure nanodrugs. However, such nanomedicines rely on the chemical structure of the drug and have so far been successfully applied to only a very limited number of drugs.

The aim of this review is to give an overview of the recent developments and applications of cylindrical drug nanocarriers, focusing on self-assembled organic devices loaded with drugs. Section 2 will summarize the current knowledge on the impact of a cylindrical shape on nanocarrier behavior upon intravascular administration. Section 3 will focus on nanocarriers in which the drug is physically loaded. They are usually generated by the self-assembly of amphiphilic block copolymers or hydrophilic peptides chemically linked to one or several alkyl chains. Section 4 will highlight bioconjugate-based nanocarriers, in which the drug is covalently coupled to an appropriate building material such as a polymer, a lipid or a peptide. Pure nanodrugs will be described in Section 5. Lastly, Section 6 will address toxicity concerns about those elongated nanocarriers.

2. General properties of cylindrical nanocarriers

Cylindrical drug nanocarriers may be encountered in the literature under the appellations nanorods, nanoworms (or worm-like particles), filomicelles, nanofibers... Those designations, mainly depending on the carrier material and on the nanocarrier stiffness are schematized in **Fig. 2**. Cylindrical nanocarriers generally display diameters below 120 nm and lengths from few hundred nanometers to several micrometers **(Table 1)**. They can be visualized by means of microscopy techniques such as atomic force microscopy (AFM), scanning (SEM), transmission (TEM) or cryogenic transmission electron microscopy (cryo-TEM) or optical (fluorescence) microscopy, depending on their size. Small-angle X-ray or neutron scattering (SAXS, SANS) may provide detailed structural information on nanocarriers in suspension in the ~ 1 – 100 nm range.[26] In addition to length and diameter, another key parameter impacting the behavior of worm-like micelles (or other flexible filamentous carriers) is their persistence length l_p, which is a measure of their flexibility. The persistence length is described as the length over which worm-like micelles are considered as rigid rods and is defined as the ratio of the bending rigidity κ and thermal energy k_BT ($l_p = \kappa / k_BT$).

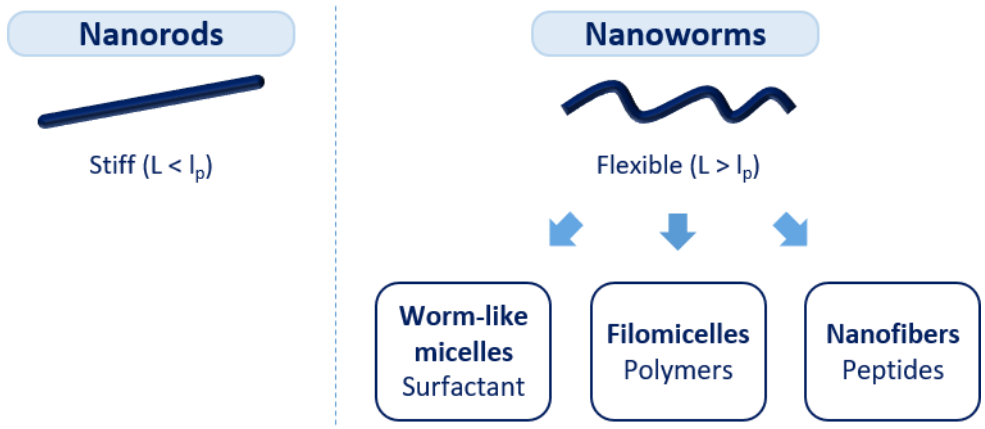

Fig. 2: Cylindrical nanocarriers and main designations based on carrier material

Table 1: Dimensions and characterization methods of the main cylindrical drug delivery nanocarriers.

System	Composition	Drug	Diameter (nm)	Length (µm)	Technique	References
Polymers	PEG-PCL	PTX	20-60	2-18	(Cryo-)TEM, Fluorescence microscopy	[8,9,27]
	PEG-PCL (silica-coated)	MTX	121	~ 1	FE-SEM	[28]
	PEG-P(CL/GA)*	PTX	20	0.1-1	TEM	[27]
	PEG-PBCL	PTX		23	Fluorescence microscopy	[25]
	PGA-*g*-(PCL-*b*-PEG)	DOX	n. d.	0.23	AFM	[29]
	mPEG-b-PDPA	SCB	19.9	50-200	TEM	[30]
	PEG-PLLA*	PTX	20	~ 0.2-> 1**	TEM, AFM	[24,31]
	PEG-PLLA*	PTX ± 17-AAG ± Rap	n. d.	> 1**	AFM	[23]
	PEG-PLA / PLA-Jeff-FA*	Betulin Derivative	n. d.	~ 0.1-1**	TEM	[32]
	Folate-PEG-PLA-PEG-Acrylate / MPEG-PLA-PEG-acrylate	DOX + SPIO	23	0.1-0.2	TEM	[33]
	LPEI-GT	DNA	53	128	AFM, TEM	[34]
	lPEI-*g*-PEG	DNA	~ 20-60	~ 0.06-1	TEM	[35]
	P(MeOx-b-BuOx-b-MeOx)	Eto ± CP	~ 50**	~ 100**	TEM	[36]
	PEG-b-PPS	ICG	50	> 1	Cryo-TEM	[37]
	PEG-PHB-PEG	ICG	5.4	> 1**	Cryo-TEM	[38]
	PEG-PHB-PEG / PF-127	ICG	5.25	~ 0.1-1**	Cryo-TEM	[38]
	$PHEMA_{122}$-*g*-(PAA_{27}-*b*-PEG_{45})	IR780	18.3	60.2	AFM	[39]
	$PHEMA_{747}$-*g*-(PAA_{21}-*b*-PEG_{45})	IR780	17.7	170.5	AFM	[39]
Peptide amphiphiles	$(C_{16}H_{32}O_2)_2$-K$(VPGAG)_3$	PTX	12-16	0.07-1.7	TEM, AFM	[40]
	qC8-Tat	PTX	15	> 1	TEM, WAXS	[41]
	KRRASVAGK[C_{12}]-NH_2	DOX	5.1	> 1	Cryo-TEM, SAXS	[42]
	C_{16}-$A_4G_3E_3$	CPT	11-12.4	> 1	TEM, SAXS	[43]

	$C_{16}V_2A_2E_2G$ ApoA1 / $C_{16}V_2A_2E_2$-NH_2	GW3965	n. d.	0.3-> 1	Cryo-TEM	[44]
	$CH_3(CH_2)_{14}$CONH-GTAGLIGQRGDS-COOH	CDDP	8-10	> 1	TEM	[45]
Polymer-drug	PGMA-*b*-POEGMA-*b*-PSt	Gd^{3+}	30	Varying with time	TEM	[46]
	PEG-TetraCPT	CPT	60	0.5	TEM, Confocal microscopy	[47]
	PEG-OctaCPT	CPT	100	1		
Lipid-drug	DLPU	Uri	~ 4.2	> 2**	SANS, SLS	[48,49]
	DLPA	Ade	~10-12	~ 0.1-> 1**	Cryo-TEM, DLS	[50]
	OA-Ara	Ara-C	n. d.	0.2-> 1**	TEM	[51]
	LA-Ara	Ara-C	~ 30	> 2**	TEM	[52]
	PA-Ara	Ara-C	n. d.	> 1**	TEM	[53]
	SQ-Dox	DOX	~ 5-6	~ 0.006-> 1**	Cryo-TEM, AFM, SAXS	[54]
Peptide-drug	Ket-L-VEVE	Ket	50.44	> 1**	TEM	[55]
	mCPT-buSS-Tau / dCPT-buSS-Tau	CPT	6.7-7.2	> 1	(Cryo-)TEM	[56]
	CPT-PTX-Sup35	CPT / PTX	7-8	> 1**	Cryo-TEM	[57]
	P18-PLGVRGRGD	P18	30	> 1**	TEM	[58]
	HCPT-MDP26 Cylinders	HCPT	14	~ 0.04	TEM, SAXS	[59]
	HCPT-MDP26 Fibers		6.8	~ 0.04		
	HCPT-MDP26-PEG		8	~ 0.05		
	DOX-KGFRWR	DOX	10.5	> 1**	TEM	[60]
	PTX-Tau	PTX	11.8	> 1	Cryo-TEM, AFM	[61]
Supramolecular hydrogels	C16V2A2E2-Nb	Nb	7	> 0.1**	TEM, SAXS	[62]
	DEX-SA	DEX	30	> 1	TEM	[63]
	PTX-SA	PTX	10-15	> 1	TEM	[64]
	CRB-FFE-YSV	CRB / YSV	30-40	> 1	TEM	[65]
	PTX-SA-NapFFKYp	PTX	29	> 1**	TEM	[66]
Pure nanodrugs	CPT / TTZ / DOX		100.8	0.63	SEM	[67]
	CPT		100-400	4-24	SEM, AFM	[68]
	HCPT / Ce6		135	0.36	SEM, TEM	[69]
	CPT-NH_2		~ 100	> 1	SEM, TEM	[70]
	SN-38		50-300	1-10	SEM, TEM	[71]

* Dimensions of filomicelles formed in a mixture of spheres and cylinders

** Extrapolated from pictures

17-AAG: Tanespimycin; AFM: Atomic Force Microscopy; BuOx: 2-butyl-2-oxazoline; DLS: Dynamic Light Scattering; Eto: Etoposide; FE-SEM: Field Emission Scanning Electron Microscopy; GT: Gelatin; GW3965: Liver X Receptor agonist; ICG: Indocyanine Green; Jeff: Jeffamine (O,O'-Bis-(2-aminopropyl) poly(propylene glycol)-*b*-poly(ethylene glycol)-*b*-poly(propylene glycol)); LPEI: Low molecular weight PEI; MeOx: 2-methyl-2-oxazoline; MPEG: methoxy-PEG; PF-127: Pluronic F-127; PPS: poly(propylene sulfide); RA: Retinoic acid; Rap: Rapamycin; SANS: Small Angle Neutron Scattering; SAXS: Small Angle X-Ray Scattering; SCB: Succinobucol; SLS; Static Light Scattering; WAXS: Wide Angle X-Ray Scattering.

Rigid nanorods under flow tend to orient along the stream lines. The order parameter *f*, which characterizes their average orientation toward the flow direction, is zero in the isotropic phase and one in the fully aligned state. It is a function of the ratio of the shear rate γ and the rotational diffusion coefficient Ω, which accounts for the nanorod random rotation due to thermal motion (Brownian motion) and increases with the shear rate and the nanorod length.[72] Long worm-like micelles also tend to align in response to flow. The behavior under shear flow of long worm-like micelles made of surfactants or amphiphilic block copolymers has been studied using SANS or SAXS, reflecting their bulk-averaged orientation correlated to a decrease in viscosity (shear-thinning rheological behavior) above a critical shear rate.[73,74] However, the reported observations of the real-time dynamics of single micelles are scarce. Disher and colleagues have visualized individual worm-like micelles, self-assembled from PEG-based block copolymers and labeled by a hydrophobic dye, using fluorescence microscopy. A flexible filomicelle could be elongated by a flow of ~ 10 μm/s in a suspension of blood cells or could be drawn from this suspension into a glass capillary, fully extending into this confining geometry.[75] In an elongational flow, PEG-PBD filomicelles exhibited a coil-stretch transition as a function of flow rate between the regime where Brownian motion dominated and the regime where the micelles were stretched and aligned by the flow. The relaxation time of filomicelles scales with their length. Consequently, for a given flow rate, filomicelles with length larger than a critical value could not relax to a random coil conformation; they extended along stream lines, whereas shorter ones did not.[76] The ability of filomicelles to stretch out within blood vessels has been invoked to explain their extended circulation.[8] This was assessed *in vitro*: in a flow chamber where the flow velocity was ~ 25 μm/s, long filomicelles evaded immobilized phagocytes whereas short cylindrical micelles and vesicles could be captured. A fraction of injected filomicelles of initial length ~ 8 μm persisted up to one week *in vivo*. Filomicelles underwent a progressive decrease in length due to cell- and flow-induced fragmentation for inert filomicelles (polyethylethylene (PEE)-PEG copolymer), combined with hydrolysis for biodegradable ones (polycaprolactone (PCL)-PEG copolymers). Persistence in circulation was shown to be strongly dependent on the filomicelle initial length, with a maximum half-life of about 5 days for PCL-PEG filomicelles of diameter ~ 60 nm and

length ~ 8 µm. As emphasized by Discher and colleagues, the ability of the fluid and flexible self-assembled filomicelles to relax and/or fragment in flow seems crucial for a prolonged circulation to occur. Indeed, they were cleared in hours when extensive cross-linking of their hydrophobic core imparted them a rigid-body behavior. This hypothesis was supported by a latter study focusing on water-soluble cylindrical polymer brushes (CPBs) consisting in a polymer backbone grafted with hydrophilic side chains. Controlled polymerization techniques allowed the tailoring of the CPB length and rigidity. The increase in rigidity of ~ 1.2 µm long CPBs resulted in more rapid clearance *in vivo* and higher deposition in the liver and spleen.[77]

In order to extravasate through vascular fenestrations, carriers need to be next to the blood vessel walls, in the red blood cells (RBC) free layer, resulting from the confinement of flowing RBCs within the core of the vessel. For a given volume fraction of RBCs (hematocrit), the thickness of the RBC-free layer depends on the blood shear rate and vessel width. The migration of spherical carriers toward the RBC-free layer relies on their interactions with RBCs. Indeed, the margination of large spherical particles in a microfluidic channel was observed only in the presence of RBCs, in agreement with simulations showing that, in the absence of RBCs, the particles follow the stream lines with no lateral drift.[78] The particle size is a crucial parameter, micrometer-sized particles displaying higher margination propensity. Using video-microscopy, Lee *et al.* have unveiled the *in vivo* distribution in mouse microcirculation of PEGylated spherical particles of polystyrene labeled with a fluorescent dye. The 200 nm particles presented a quite uniform radial distribution, without preferential near-wall accumulation. In contrast, the 1000 nm particles experienced migration into the RBC-free layer.[79] These findings are consistent with numerical simulations performed with different models, suggesting that particles with diameter smaller than ~ 100 - 250 nm moved with RBCs whereas particles with diameter larger than ~ 500 - 1000 nm were pushed toward the vessel walls.[80] Regarding the effect of flow rate, Carboni *et al.* revealed the increase in margination with increasing flow rate by direct tracking of fluorescent particles flowing through a microfluidic channel.[78] This experiment was also consistent with results from simulation studies. The particle shape is also expected to play a key role because the forces and torque exerted on the particles in the blood stream depend on their shape. Non-

spherical particles may undergo tumbling and rolling, affecting their trajectory and probability of contact with the walls. It should be noted that in experimental studies the margination of rigid rods was not measured independently from their adhesion to the wall of a microfluidic device. Mitragotri's group has compared the adhesion of rod-shaped and spherical polystyrene particles of equal volumes in either a synthetic microvascular network or a parallel plate flow chamber, with or without RBCs.[81–83] The fluid shear rates were typical of those observed in the microcirculation. Adhesion was facilitated by specific ligand - receptor interactions between the functionalized particles and walls (*e.g.* biotin - avidin or bovine serum albumin (BSA) - anti-BSA monoclonal antibody interactions). The key finding was that rod-shaped particles with lengths in the ~1 – 10 μm range exhibited higher adhesion / retention, due to larger contact area and lower drag force exerted by the fluid flow. Moreover, the difference between the adhesion / retention of rods and spheres of equal volumes was enhanced for larger particles, highlighting the interplay between size and shape. Interestingly, Vahidkhak and Bagchi have emphasized in a simulation study that the shape of the microparticles affected their margination and wall adhesion behaviors in the blood flow differently. Rod-shaped microparticles displayed a lower near-wall accumulation compared to spherical microparticles but a higher overall probability of adhesion, in agreement with experimental findings.[84] Very few studies have dealt with margination / adhesion of flexible worm-like micelles.[85] But Shuvaev *et al.* have investigated polymeric filomicelles decorated with high affinity antibodies targeted to surface molecules of lung endothelial cells. They have shown that these filomicelles, about 7.5 μm in length, could combine their preserved ability to circulate for a long time with efficient and specific binding to endothelial cells *in vivo*, despite the large drag from the flow.[86]

Nanocarriers must then penetrate the tumor interstitial matrix, comprising mainly collagen, to deliver a drug to the target cancer cells. Porous collagen or agarose gels have been used to model *in vitro* the transport of nanocarriers across vessel pores and their diffusion into tumors. Chauhan *et al.* have compared the penetration of inorganic nanorods and nanospheres coated by a PEG layer into collagen gels. The two nanocarriers had the same 33-35 nm hydrodynamic diameters and, consequently, nearly identical diffusion rates in water. However, nanorods diffused through the gels

about 5 times faster than the nanospheres. In another experiment, it has been also suggested that the transport rate through the pores depended strongly on the nanocarrier diameter.[87] As demonstrated by Kim *et al.*, polymeric filomicelles with a mean contour length of ~ 6.8 μm and a diameter of ~ 25 nm were able to permeate under a solute density gradient through the 100 nm pores of an agarose gel. In contrast, 100 nm sized polymeric vesicles remained at the solution / gel interface.[88] The filomicelle radius of gyration exceeded half the size of the gel pores but flexible, loosely coiled, filomicelles could extend to reptate through the gel.[89] The above mentioned nanorods and filomicelles accumulated more efficiently in tumors *in vivo* than their spherical counterparts, in agreement with *in vitro* experiments. Shukla *et al.* have further investigated the influence on the tumor homing properties of the aspect ratio of rigid nanorods formed by self-assembly of the tobacco mosaic virus (TMV) coat protein. TMV-based nanorods with 18 nm diameter and different aspect ratios (3.5, 7 and 16.5) were achieved and their surface functionalized with PEG. The smallest nanorods (18 x 63 nm) showed higher tumor penetration and accumulation, despite a shorter circulation time.[90]

Nanocarriers are internalized in non-phagocytic cells *via* endocytic pathways divided into macropinocytosis, clathrin-mediated endocytosis, caveolae-mediated endocytosis and clathrin- and caveolae-independent endocytosis. The preferred pathways are suggested to depend on the properties of the particles and the nature of the cell lines.[91–93] Regarding the influence of shape on the extent and kinetics of nanocarrier uptake, no clear picture could emerge. This is probably due to the difficulty to separate the shape effects from those of other parameters (size, elasticity, charge and surface chemistry).

Molecular simulations performed by *Li et al.* suggested that rod-like nanocarriers are less efficiently internalized than their spherical counterparts due to the larger bending energy of a membrane wrapping around a cylindrical nanoparticle.[94] Experiments on the uptake of gold nanoparticles into HeLa cells might be partly explained by these findings. Cellular uptake of rods was lower than that of spheres and further decreased when the aspect ratio increased.[95]

On the other hand, it is interesting to note that a rod-like shape can enhance the role of ligands concerning the cellular uptake since it provides larger surface areas of contact between the nanoparticles and the cell membrane. Barua *et al.* have investigated the uptake of spherical and rod-shaped polystyrene particles of two sizes (200 nm and 1 μm) in three breast cancer cell lines. Rod-shaped particles were prepared from spherical particles using the film-stretching process, thus ensuring that they have the same volume. Whereas uncoated nanorods exhibited lower uptake compared with spheres, they showed significantly higher uptake after coating with trastuzumab as a targeting antibody (TTZ). This effect was more prominent for microparticles than for nanoparticles. This model system demonstrates that particle shape can significantly improve the specificity of the binding and the uptake into cancer cells.[96] This approach was further successfully applied to the targeting of other types of endotheliums, such as lung [81], brain [81,97] or gastrointestinal tract [98,99] by polystyrene nanorods coated with targeting ligands. Thus, all of these studies evidenced that coated polystyrene nanorods achieved a much higher accumulation into the targeted endothelium than both their spherical counterparts and the nanorods coated with non-specific immunoglobulin G, hence confirming the pertinence of cylindrical nanocarriers towards a wide range of applications.

These results are consistent with those reported by Gratton *et al.* Using the PRINT method, they have designed a series of PEG hydrogel particles and examined the shape effects on the cell internalization by comparing HeLa cell endocytosis of cubic and cylindric particles of various sizes. Rod-like particles were internalized faster and to a larger extent than cubic-shaped particles, through various mechanisms of endocytosis. Furthermore, the rate of internalization was increased for cylinders having similar volumes upon increasing their aspect ratio. This was tentatively attributed to the interactions of the positive charges of the particles with the cell membrane.[100]

Other examples of enhanced cellular uptake for rod-like or worm-like nanoparticles compared to spherical ones include nanoparticles formed by polymerization-induced self-assembly (PISA) of amphiphilic copolymers [101] and nanoparticles formed by self-assembly of dendritic polymer-drug conjugates.[102]

Taken together, the above studies on model systems suggest that cylindrical nanocarriers should be more effective than spherical ones for active targeting of the endothelium and anticancer drug delivery. Among them, long and flexible filomicelles display unique properties, differentiating them from shorter rigid nanorods. In addition to long circulation time, they can extravasate through vessel pores due to their small diameter and reptate deeply into tumors owing to their flexibility, while enabling a drug payload typical of microsized carriers. The anticancer properties of various cylindrical nanocarriers compared to those of their spherical counterparts are reported in **Table 2**, pointing to improved therapeutic outcome.

3. Drug-loaded nanocarriers

Drug-loaded nanocarriers refer here to nanomedicines consisting in a drug physically entrapped into a nanovector either in its core or at the surface, depending on the properties of both the drugs and the carrier material. Compared to the chemical encapsulation, this approach seems simpler as it doesn't require difficult chemical step to synthesize nanomedicines-forming bioconjugates. However, it is necessary to investigate the encapsulation efficiency, as the presence of a proportion of remaining free drug in the suspension may require an additional purification step to avoid any related toxicity or side effects. Furthermore, structural characterization of drug-loaded nanocarriers is essential as the incorporation of drugs may impact the physico-chemical characteristics of the nanomedicines, or change their morphology.[103]

Table 2: Anticancer properties of cylindrical nanocarriers compared to their spherical counterparts.

Cylinder composition	Sphere composition	Drug	IC50	Cell lines	Maximum tolerated dose	Other	References
PEG-PCL	PEG-PCL	PTX	~	A549	↗ x ~ 2	~ drug release rate in buffers in DPBS (pH 7.4) and DPBS:FBS 1:1 ~ tumor apoptosis ↘ nontumor organs apoptosis ↘ A549 tumor growth	[8–10,104]
PEG-PCL (silica-coated)	PEG-PCL (silica-coated)	MTX	↘ / 1.1	MCF-7	n. d.	↘ drug release rate over 160 h in PBS (pH 7.4)	[28]
PGA-*g*-(PCL-*b*-PEG)	PEG-PCL	DOX	↘ / 1.6	EJ	n. d.	↗ drug release over 110 h in PBS (pH 7.4) ↗ cell uptake by HeLa and HepG2 cells	[29]
PEG-TetraCPT/DOX	PEG-DiCPT/DOX	CPT	↘ / 2 ↘ / 1.7	MCF-7 MCF-7/ADR	n. d.	↗ blood circulation time ($t_{1/2}$ ↗ x 3.6) ↗ tumor accumulation	[102]
PEG-OctaCPT/DOX	PEG-DiCPT/DOX	CPT	↘ / 1.9 ↘ / 1.7	MCF-7 MCF-7/ADR	n. d.	~ blood circulation time	[102]
POEGMA-*b*-P(ST-*co*-VBA)/DOX Worms	POEGMA-*b*-P(ST-*co*-VBA)/DOX	DOX	↘ / 7.3 (Worms) ↘ / 2.8 (Rods)	MCF-7	n. d.	↗ cell uptake ~ drug release rate over 72 h in buffers (pH 5.0 and 7.4)	[101]
HCPT / C18PMH-PEG	HCPT / C18MPH-PEG	CPT	↘ / 2 ↘ 1.7 ↘ 1.4	KB 4T1 MCF-7	↘ / ~1.6	↘ drug release rate over 70 h in PBS (pH 7.4) ↗ and faster uptake by KB cells ↗ blood circulation time ~ accumulation in 4T1 tumor ↘ 4T1 tumor growth	[105,106]
MTX-PEG-CPT	MTX-PEG-CPT	MTX / CPT	↘ / 1.9	HeLa	n. d.	~ drug release over 48 h in PBS (pH 7.4) ↗ and faster uptake by HeLa cells ↗ blood circulation time ($t_{1/2}$ ↗ x 1.8) ↗ accumulation in HeLa tumor	[107]

Gem-5-isoprene	Gem-Sq	Gem	↗ x 2 ~	MiaPaCa-2, B16F10, CCRF CEM MCF-7, A549, L1210wt	n. d.	↘ uptake rate in MiaPaCa-2 and B16F10 cells over 4 h	[108]

↗: increase; ↘: decrease; ~: comparable

FBS: Fetal Bovine Serum.

3.1. Polymer-based nanocarriers

Most of the cylindrical polymeric nanocarriers rely on the self-assembly in water of amphiphilic diblock copolymers involving a PEG chain, on one hand, and a polyester chain such as PCL or PLA, on the other hand. The hydrophilic, FDA approved PEG, is biocompatible and able to reduce opsonization, conferring stealth properties to the nanoassemblies. PCL and PLA are hydrophobic, biocompatible and biodegradable polymers widely used in biomedical applications. Two methods are broadly used to induce the self-assembly of amphiphilic copolymers in water. In the thin-film hydration method, water is added under stirring on a film obtained by drying a solution of the copolymer. The second method involves the addition of water to a solution of the copolymer in an organic solvent (or the reverse). The solvent is then removed by evaporation or dialysis.[109]

The free energy of the self-assembly determines the thermodynamically stable morphology of the core-shell nanocarrier. For amorphous copolymers, it depends on the degree of stretching of the hydrophobic core chains, the interfacial tension between the core and water, and the repulsive steric interactions between PEG corona chains. The key parameter is the PEG weight fraction (f_{EO}), as shown by extensive studies on PBD-PEG and PEE-PEG copolymers. Self-assembly interfacial curvature increased with increasing f_{EO}, inducing shape transitions from bilayers to cylinders thento spheres. In dilute solutions, wormlike micelles were observed alone over a relatively narrow range of PEG weight fractions ($\sim 0.3 < f_{EO} < 0.55$). They coexisted with either vesicles or spherical micelles in the wider vesicles/ wormlike micelles and wormlike micelles/ spherical micelles boundary regions, respectively.[24,109–112]

This conventional phase behavior of amorphous block copolymers as a function of the hydrophilic weight fraction can be modified by the crystallization of the core-forming blocks such as PCL or poly(L-lactide) (PLLA) blocks, due to the contribution of crystallization to the self-assembly free energy. Crystallization may favor the formation of cylindrical micelles because of their lower interfacial curvature, compared to spherical micelles **(Fig. 3)**.[113,114] For example, it has been shown that core crystallization could induce the formation of rods upon aging of initial amorphous

spherical micelles of PCL-PEG (CL_{26}-$E0_{45}$) copolymer.[115] Kim *et al.* have also reported the unexpected formation of filomicelles at f_{EO} ~ 0.8, using the PEG-PHB-PEG copolymer which contains the highly crystalline isotactic poly((R)-3-hydroxybutyrate) (PHB) hydrophobic block.[38] As another example, PEG-based amphiphilic copolymers with either crystalline poly(caprolactone-*b*-L-lactide) (P(CL-LLA)) or amorphous poly(caprolactone-*b*-D,L-lactide) (P(CL-DLLA)) as the hydrophobic block formed cylindrical or spherical micelles, respectively.[116] Other studies dealing with PCL- or PLA-based copolymers have highlighted the effect of the regularity of the hydrophobic chain structure and of the lengths of both blocks on the formation of either worm-like or spherical micelles, with similar f_{EO}. Jelonek *et al.* have investigated the influence of the stereochemistry of the PLA block on the self-assembly of PLA-PEG copolymers. PLLA-PEG ($LLA_{85}EO_{114}$, f_{EO} ~ 0.45) copolymer mainly formed filomicelles, whereas PDLLA-PEG ($DLLA_{81}EO_{114}$, f_{EO} ~ 0.46) copolymer, displaying L-lactide and D-lactide units randomly distributed along the chain, formed only spherical micelles.[24] Sun *et al.* have shown that the introduction of even small amounts of glycolide (GA) units in the PCL chains perturbed the chain structure and led to the formation of spherical micelles instead of PCL-PEG filomicelles.[27]

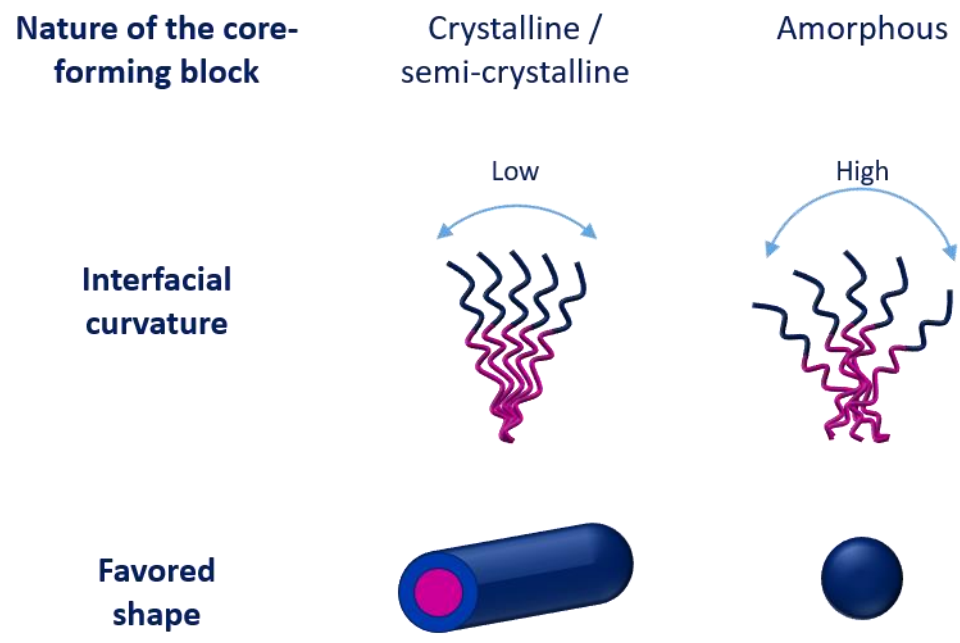

Fig. 3: Role of the crystallinity of the core-forming block polymer on the shape of nanoparticles.

Crystallization tends, therefore, to rigidify the wormlike micelle core. However, flexibility is an essential feature for long circulating properties. Flexible wormlike micelles could be obtained with PCL-PEG copolymers, despite the propensity of PCL chains to crystallize. Crystallization was suppressed for low molecular weight PCL blocks because the high core curvature could induce defects hindering the regular stacking of PCL chains, thus leading to the formation of flexible filomicelles. Crystallization was also prevented in high molecular weight PCL blocks by random copolymerization with racemic lactide units, disrupting the ordered chain packing.[113]

An alternative approach sometimes used to achieve wormlike morphology is to synthesize CPBs, composed of a chain backbone densely grafted with side chains. The steric repulsion between neighboring side chains causes extension of the chain backbone; longer side chains and higher grafting degrees lead to more elongated shapes and wormlike morphology of the unimolecular micelle which is obtained for high aspect ratio of the backbone and side chains.[117] When the side chains are amphiphilic copolymers a core-shell structure may be obtained. And antibodies may even be bound to the side chains for specific cell targeting. But few examples of biomedical applications are reported so far. They include CPBs carrying doxorubicin [29], CPBs complexing DNA or siRNA [35,118] and CPBs binding the cationic IR780 molecule through electrostatic interactions for photothermal cancer therapy [39].

The core of filomicelles can carry hydrophobic drugs. The drug loading can be performed by two methods: (i) either the drug is solubilized into the organic phase, prior to the formulation of the nanocarrier, (ii) or the empty nanocarrier is formulated and the drug loaded *a posteriori* by incubation of the nanocarrier suspension with a drug-containing solution. The drug loadings of different cylindrical polymer nanocarriers are gathered in **Table 3**. They are compared to those of the corresponding spherical micelles when data are available. They are usually higher, as expected, because a cylindrical micelle has a larger volume to surface area ratio than *n* spheres of the same radius and same total mass.[119] Drug loading also increases with the radius of the micelle core, depending on the length of the copolymer hydrophobic block. Of note, drug loading may also be affected by the amorphous or crystalline nature of the core.

Table 3: Drug loading of polymeric nanocarriers

Filomicelles composition	Spheres composition	Drug	Filomicelles drug loading (%)	Compared to spheres		References
				Drug loading	Loading efficiency	
PEG-PCL	PEG-PCL	PTX	~ 2.9-4.7*	↗ (x ~ 2)	↗ (x ~ 2)	[9]
PEG-PCL	PEG-P(CL-GA)	PTX	10.6-12.4	↘ (~-2.5 %)*	↘ (~-15.1 %)*	[27]
PEG-PCL (silica-coated)	PEG-PCL (silica-coated)	MTX	3.5	↗ (+ 1.4 %)*	↗ (+ 39.4 %)*	[28]
PEG-PBCL	n. d.	PTX	~ 3.2*	n. d.	n. d.	[25]
PGA-*g*-(PCL-*b*-PEG)	PEG-PCL	DOX	3	↘ (- 2.9 %)*	↘ (- 25 %)*	[29]
mPEG-b-PDPA	n. d.	SCB	15.6	n. d.	n. d.	[30]
PEG-PLLA	PEG-PDLLA	PTX	4.9-11.3	↗ (+ 1.5 %)*	↗ (+ 17.1 %)*	[24,31]
PEG-PLLA	n. d.	PTX ± 17-AAG ± Rap	3.1-4.6 2.1-4.7 1.4-1.8	n. d.	n. d.	[23]
PEG-PLA / PLA-Jeff-FA	n. d.	Betulin derivative	19.7-20	n. d.	n. d.	[32]
FA-PEG-PLA-PEG-Acrylate / MPEG-PLA-PEG-acrylate	n. d.	DOX + SPIO	9 48	n. d.	n. d.	[33]
LPEI-GT	n. d.	DNA	3.8*	n. d.	n. d.	[34]
lPEI-*g*-PEG	n. d.	DNA	n. d.	n. d.	n. d.	[35]
P(MeOx-b-BuOx-b-MeOx)	n. d.	Eto ± CP	16.2-~ 50 19.2-36.2	n. d.	n. d.	[36]
$PHEMA_{122}$-*g*-(PAA_{27}-*b*-PEG_{45})	$PHEMA_{57}$-*g*-(PAA_{21}-*b*-PEG_{45})	IR780	24.5	~ (- 0.1)	~ (- 0.6)	[39]
$PHEMA_{747}$-*g*-(PAA_{21}-*b*-PEG_{45})	$PHEMA_{57}$-*g*-(PAA_{21}-*b*-PEG_{45})	IR780	24.7	~ (+ 0.1)	~ (+ 1.3)	[39]

* Calculated from data

↗: increase; ↘: decrease; ~: comparable

The delivery using filomicelles of paclitaxel (PTX), a hydrophobic anticancer drug with a very low water solubility, has been widely investigated by Discher's group [120] and Jelonek *et al.*[23,24]. Discher and colleagues have found that PTX could spontaneously partition into the hydrophobic core of PCL-PEG filomicelles. Two copolymers with similar f_{EO} ~ 0.42-0.43 but different molecular weights, either Mn ~4700 ($CL_{24}EO_{45}$) or Mn ~ 11500 ($CL_{57}EO_{114}$), were studied. The drug loadings were 4.5 and 6.7 wt. %, respectively, consistent with the larger core diameter of PCL-PEG 11500 (d = 29 nm) than PCL-PEG 4700 (d = 11 nm).[119] It was further demonstrated that linking a benzyl group to the PCL chain increased the solubilization of PTX, which displays multiple aromatic moieties, into the filomicelle core. The PTX loading capacity of PEG-poly(α-benzyl carboxylate ε-caprolactone) (PBCL-PEG) filomicelles was improved by 40% over PCL-PEG filomicelles.[25] Discher's group have also recently shown that PCL-PEG filomicelles could deliver a combination of PTX and retinoic acid for the treatment of liver cancer models, more effective than free drugs or separately loaded drugs.[121] PTX could also be incorporated into PLLA-PEG filomicelles with a comparable loading content, in the 4.7 - 6.5 wt. % range for an initial amount of drug of 10 wt. %, depending on the copolymer molecular weight. Longer PLLA and PEG blocks ($LLA_{85}EO_{114}$) led to higher encapsulation.[24] PTX was further loaded in PLLA-PEG filomicelles with either a heat shock protein 90 inhibitor (17-AAG) alone or a mixture of 17-AAG and rapamycin (Rap) by a one-step physical process. PTX and 17-AAG presented similar loadings in PTX / 17-AAG loaded filomicelles (3.1 ± O.6 and 3.7 ± 1.5 wt. %, respectively). In contrast, in PTX / 17-AAg/Rap loaded filomicelles, higher incorporation of PTX was observed compared to 17-AAG and Rap, the latter having the lowest loading content (4.6 ± 1.4, 2.7 ± 0.2 and 1.8 ± 0.3 wt. %, respectively). These differences reflected interactions of drugs with PLA-PEG and with each other.[23]

The drug loading in filomicelles remains generally quite low, in the 5 - 10% range. However, the triblock amphiphilic copolymer poly(2-methyl-2-oxazoline-*b*- 2-butyl-2-oxazoline-*b*- 2-methyl-2-oxazoline) was recently shown to form wormlike nanocarriers with an exceptional drug loading, superior to 50 % for the combination of etoposide (ETO) and an alkylated cisplatin prodrug (C_6CP), displaying synergistic effects against lung cancers.[36] This remains, to date, the wormlike-forming

copolymer with the highest drug loading capacity. Remarkably, the loading of ETO promoted the formation of short worms, with an aspect ratio of 1.5-2, in coexistence with spherical micelles. This elongated morphology was preserved upon co-loading of ETO and C_6CP, whereas micelles loaded only with C_6CP were spherical, highlighting the importance of specific drug-polymer interactions.

Drug release from filomicelles may occur through passive diffusion and/or degradation of the core. After an initial burst release, a sustained release of PTX from PCL-PEG and PLLA-PEG filomicelles was observed *in vitro*. In both cases, the prolonged PTX release could be correlated to the degradation of the filomicelles. The initial burst release of PTX, ~ 50 % within 1 h for filomicelles of PCL-PEG with molecular weight Mn ~ 4700 ($CL_{24}EO_{45}$), was suggested to result from the drug molecules located at the core-corona interface. The remaining PTX was then released over 36 h with an almost constant rate. The concurrent degradation of PCL-PEG filomicelles at 37 °C in buffer was monitored by gel permeation chromatography (GPC), revealing a new species that was found to be the monomer product of PCL hydrolysis (6-hydroxycaproic acid, 6-HPA). Hydrolysis took place by chain-end cleavage, resulting in a progressive reduction of the PCL block length and an increase in the f_{EO} ratio. This induced a gradual transition from worm-like to spherical micelles and the shortening of filomicelles, as shown by fluorescence microscopy and cryo-TEM.[119,122] The time required for the completion of the morphological transition was ~ 28 h, underlining the relationship between filomicelle degradation and PTX release. Degradation kinetics was found to depend on temperature, pH and molecular weight Mn of PCL-PEG. It was minimal at 4 °C, increased at acidic pH (pH 5), consistent with acid-catalyzed ester hydrolysis, and strongly decreased for Mn ~11500 ($CL_{57}EO_{114}$). PLLA-PEG ($LLA_{85}EO_{114}$) filomicelles revealed a much slower PTX release, of the order of 10 % after 71 days at 37 °C in PBS at pH 7.4. The PTX release kinetics was further compared to the degradation of filomicelles in the same conditions. The decrease in molar mass of PLLA-PEG ($LLA_{85}EO_{114}$) block copolymer was measured by GPC and the increase in EO/LLA ratio by NMR, supporting the correlation between filomicelles degradation and drug release. Of note, a significantly higher drug release was observed for PDLLA-PEG ($DL_{80}EO_{114}$) spherical micelles (~ 30, 33 and 63 % at pH 7.4, 5.5 and 3.0, respectively) compared to PLLA-PEG filomicelles (~ 10, 15 and 22 % at pH 7.4, 5.5 and

3.0, respectively). This was correlated to the amorphous nature of the spherical micelles core.[31] This degradation-coupled release of the drug, enhanced at low pH, is particularly interesting regarding cancer therapy, since pH is lower in tumor tissues than in healthy ones.

Thus, wormlike micelles with pH-responsiveness have been specifically designed to be activated in acidic environments. For example, the poly(2-diisopropyl methacrylate)-b-PEG (PDPA-b-PEG) copolymer and the Y-shaped copolymer consisting of one PEG block and two 3-diethylaminopropylated poly(L-lysine) (poly(Lys-DEAP)) blocks were synthesized and shown to self-assemble as filomicelles.[30,123,124] Their hydrophobic blocks contain amine groups whose protonation at acidic pH will turn them hydrophobic to hydrophilic, causing the disassembly of the filomicelles, hence triggering the release of the encapsulated drug. This feature helps targeting solid tumors, based on the slightly acidic pH of their extracellular environment (~ pH 6.8), for (poly(Lys-DEAP))$_2$-PEG [124], or enables drug release in late endosomes (~ pH 5.5) or lysosomes (~ 4.7) of cancer cells for PDPA-b-PEG.[30,123]

Polyester-based filomicelles were also successfully used for theranostic purposes. Yang *et al.* developed a multifunctional cylindrical nanovector obtained from a mixture of PEG-PLA-PEG-acrylate and folate-PEG-PLA-PEG-acrylate polymers, for the encapsulation of the anticancer drug doxorubicin (DOX) together with Small Particles of Iron Oxide (SPIO) as magnetic resonance imaging (MRI) contrast agent.[33] Folic acid (FA) allowed active cell recognition, as folate receptors are overexpressed on the cell surface of a wide range of human carcinomas [125], while acrylate groups were introduced to allow crosslinking of the inner PEG layer, conferring enhanced stability to the nanocarrier and sustained doxorubicin delivery.

3.2. Peptide amphiphiles

Peptide amphiphiles (PAm) are basically constituted of a biologically active hydrophilic peptide chemically coupled to one or several alkyl chains. Alkyl chain and peptide must be carefully chosen to optimize the properties of the formed nanofibers. Due to their hydrophobic nature, the alkyl

tails tend to aggregate in water, forming the nanofibers core to restrict contact with the aqueous environment. This is the driving force of the self-assembly process. Simultaneously, the nature and conformation of the peptide headgroup influences the size and shape of the nanoassemblies: peptides in α-helixes or random coil conformation may form either spherical or cylindrical micelles, while peptides forming β-sheets will exclusively form nanofibers.[126] The β-sheet role in the formation of elongated structures was investigated in detail by Paramonov *et al*.[127] After screening 26 amphiphilic peptides composed of a palmitic C_{16} chain linked to the peptide headgroup *via* a glycine-based linker, the authors highlighted the necessity for the four amino acids located the closest to the nanoparticle core to be able to form β-sheet hydrogen bonds with neighboring peptides to allow the formation of nanofibers. To go further, Tirrell group focused few years later on the self-assembly mechanism of worm-like PAm through the example of a conjugate made of a C_{16} alkyl chain linked to three tryptophan and one lysine units (C16-W3K). Notably, the possibility was demonstrated to initiate a transition from sphere to rod by triggering a transition in the peptide conformation from α-helixes to β-sheets after heating. The growth mechanism was shown to occur through the attachment of transient spherical micelles to the end of the growing cylindrical micelles upon heating **(Fig. 4a)**.[128,129] With successive developments, additional structural region can be added to the initial alkyl core and β-sheet-forming moieties, like a third segment composed of a sequence of amino acids designed to allow structural modifications (improve water solubility, trigger gelation…) and possibly a fourth domain consisting in a sequence incorporating a bioactive signal, like cell adhesion for example or a therapeutic molecule. **(Fig. 4b, c)**.[130,131]

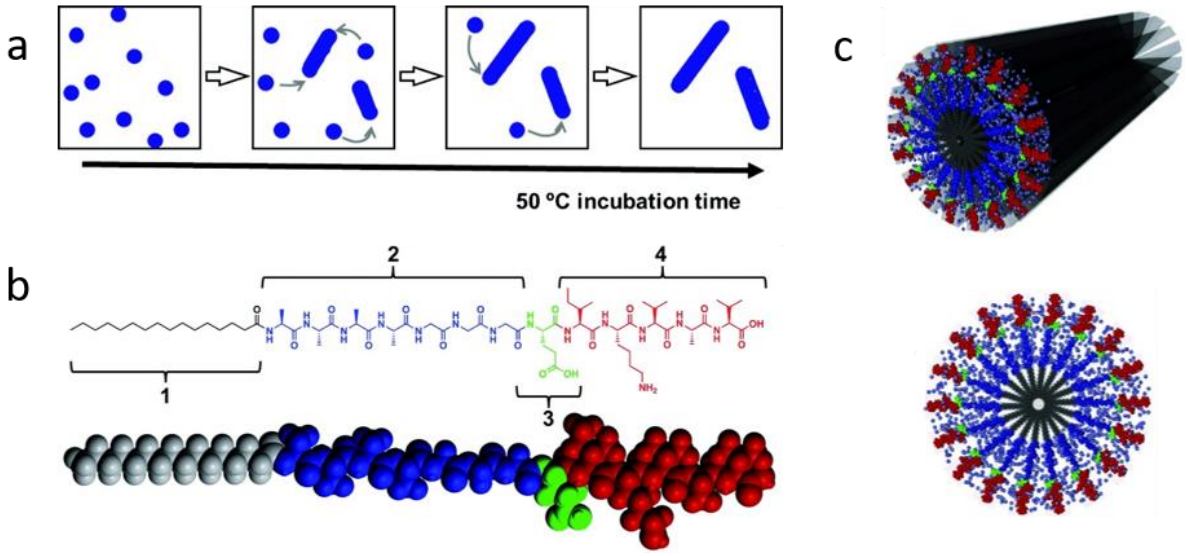

Fig. 4: (a) Self-assembly process of worm-like micelle in the PAm C16-W3K during the 50°C incubation; (b) Molecular structure of a representative peptide amphiphile with four rationally designed chemical entities; (c) Molecular graphics illustration of the peptide amphiphile molecule and its self-assembly into nanofibers, as well as, an illustration of the cross section of these fibers, highlighting the extensive hydration of the peptide shell. Adapted with permission from [129,130].

The formulation process of drug loaded amphiphilic peptide nanofibers is straightforward as they spontaneously self-assemble after hydration with usually water or PBS at pH 7.4. Small anticancer drugs can be loaded into the nanofibers core by mixing the drug and PAm, prior to the hydration step, in a strong solvent like hexafluoro-2-propanol to allow molecular mixing. The obtained mixture is then evaporated to complete dryness before hydration with water or a buffer to obtain the self-assembled structures.[40,41,43,44,132] The drug loading into such peptide-based nanofibers is, unfortunately, rarely mentioned in the literature. However, Soukasene *et al*. reported a molar ratio of 1:28, between the encapsulated drug, here camptothecin (CPT), and the peptide nanocarrier [43], while in another study Tat-based nanofibers loaded with PTX revealed a drug content of 6.8 %, which may be considered as a high loading capacity for elongated nanoassemblies.[41] The rationale was to design PAm nanofibers with multiple short C_8 tails rather than with a single one to widen the core and reduce its crystallinity, hence allowing the incorporation of more hydrophobic drug. And effectively, the 4-tail conjugate incorporated more drug than the 1-tailed and 2-tailed counterparts. Of note, the carrier rigidity generally increased with the drug loading, as another potential way to control the physico-chemical properties of the nanocarriers and to modulate their behavior after administration.

Interestingly, the length of PAm nanofibers may be adjustable. For example, addition of various amounts of the capping phospholipid 1,2-dioleoyl-sn-glycero-3-phosphoethanolamine (DOPE) to the elastin-based PAm nanofibers stopped their growth by forming endcaps: nanofibers length decreased in a controlled way when increasing the DOPE amount, without alteration of the fibers diameter.[40] Since the length of nanofibers is largely involved in the biological processes, this study could provide a simple mean to modulate the therapeutic response of the drug loaded into the PAm nanofibers.

PAm as nanocarriers have mainly been applied to cancer treatment: after loading of anticancer drug, they generally exhibited an increased *in vitro* toxicity against several lines of breast cancer cells compared to the free drug, along with a reduction of the tumor volume *in vivo*.[42,43,132] Similarly to polymeric filomicelles, stimuli-sensitive PAm could be designed to release drug in a controlled way. Specific sequences substrate of enzymes like matrix metalloproteinase-2 (MMP-2) [45] or protein kinase A (PKA), both overexpressed in various cancers, can be incorporated into the amino acids sequence of the peptide to specifically trigger the drug release into the tumor.[42,45] A first strategy was to insert the MMP-2-sensitive sequence between the alkyl chain and an RGDS epitope (used for recognition). After complexation with cisplatin (CDDP), the enzymatic degradation resulted in the cleavage of the PAm, triggering the release of CDDP-RGDS complexe. In another way, the insertion of a sequence sensitive to PKA led to a completely different mechanism: the phosphorylation of the substrate by PKA caused the disruption of the nanofibrous structure without destroying the PAm, hence allowing the release of the encapsulated doxorubicin in the presence of cancer cells. The reverse reaction, dephosphorylation by alkaline phosphatase, allowed then the reversible formation of the nanofibers.[42] Recently, PAm nanofibers were adapted to treat atherosclerosis. The design of nanofibers made of apolipoprotein-mimetic peptides permitted a specific accumulation into the atherosclerotic plaques in a model of LDLR KO mice and an improved cholesterol efflux from macrophages after loading the fibers with liver X receptor agonist.[44]

Under specific conditions, Pam nanofibers may also entangle to form hydrogels. Practically, the peptide headgroup can be functionalized by small molecules such as hydrogelators, allowing the gelation of the PAm suspension after screening the electrostatic repulsive forces, generally by the

addition of a counterion.[62] And the encapsulated drug itself can be also used as the screening agent. For instance, CDDP loading into PAm suspension was found to induce gelation by forming inter-fiber complexes between the carboxylic acids of the peptide headgroups and the CDDP. Unexpectedly, this hydrogel displayed a high drug release *in vitro*, up to 80 % after 24 h at pH 7.4.[45] More recently, a gel was designed by the co-assembly of positively charged Lauryl-VVAGEE PAm and negatively charged Lauryl-VVAGKKK-AM PAm for DOX encapsulation. The drug release rate *in vitro* could then be adjusted by varying the initial PAm concentration. Prolonged drug delivery resulted in tumor growth and tumor volume reduction in 4T1 tumor-bearing BALB/c mice.[132] The potentialities of controlling the gelation as well as the drug release, along with the mechanical properties of the hydrogel, make them interesting candidates also for the development of prolonged local drug delivery systems.

4. Bioconjugate-based nanocarriers

Chemical drug loading relies on the covalent linkage of a drug to an appropriately chosen building material. This approach led to the development of an important variety of one-component nanomedicines. Among the numerous advantages of these drug delivery systems, one can cite a dramatic increase of the drug content **(Table 4)** - and thus a reduced amount of inert material to be administered to the patients -, an improved solubility of the drug, the prevention of potential burst release and a better bioavailability.[133,134]

Table 4: Drug loading of prodrug nanocarriers

System	Composition	Drug	Drug loading (%)	References
Polymers-based	PEG-TetraCPT	CPT	30.6	[102]
	PEG-OctaCPT	CPT	38.9	[102]
	POEGMA-b-P(ST-co-VBA)	DOX	5.0	[101]
Lipid-based	DLPA	Ade	32.6*	[50]
	DLPU	Uri	30.6*	[135]
	OA-Ara	Ara-C	47.9*	[51]
	LA-Ara	Ara-C	57.3	[52]
	PA-Ara	Ara-C	50.4*	[53]
	SQ-Dox	DOX	57.0	[136]
Peptide-based	Ket-L-VEVE	Ket	33.4*	[55]
	CPT-buSS-Tau	CPT	23-31	[56]
	CPT-PTX-Sup35	CPT	29	[57]
		+ PTX	12	
	DOX-KGFRWR	DOX	31.9*	[60]
	PTX-buSS-Tau	PTX	41.0	[61]
	dCPT-K2	CPT	43	[137]
	dCPT-OEG_5-K2	CPT	36	[137]
	dCPT-Sup35-K2	CPT	28	[137]
Supramolecular hydrogels	DEX-SA	DEX	77.0*	[63,138]
	PTX-SA	PTX	87.9*	[64]
	CRB-FFE-YSV	CRB	26.7*	[65]
		+ YSV	34.0*	
	TA-SA-Glu	TA	62.3*	[139]

* Calculated from data

4.1. Polymer-based conjugates

Two approaches exist to develop drug-polymer filomicelles. The first method consists in using the drug molecule itself as one of the material building blocks. For example, Zhou *et al*. have chosen to exploit the hydrophobic nature CPT and have synthesized PEG_{45}-b-dendritic polylysine-camptothecin (PEG_{45}-xCPT) conjugates.[102] They discovered that by carefully choosing both the number of CPT molecules linked to dendritic polylysine (DPLL) moieties and the number of the dendritic generations altered the conjugate amphiphilicity, enabling to obtain various nanostructures. More precisely, the conjugates with four and eight CPT molecules (PEG_{45}-TetraCPT and PEG_{45}-OctaCPT, respectively) allowed to obtain nanorods with drug content of 30.6 % and 38.9 %, respectively, while assemblies with one or two CPT molecules only displayed spheres with drug loadings of 13.4 % for PEG_{45}-CPT and 21.4 % for PEG_{45}-DiCPT. Such aggregates were formed by a simple procedure: briefly, deionized water was added dropwise under stirring into a filtered solution of PEG_{45}-xCPT in *N*,*N*-dimethylformamide (DMF). The DMF was then removed by dialysis. The obtained PEG_{45}-TetraCPT nanorods dimensions were ~ 60 nm diameter and 500 nm length, while the PEG_{45}-OctaCPT were bigger: ~ 100 nm diameter and 1 µm length. TEM observations revealed rigid rods, as a consequence of the hydrogen bonding between DPLL amide groups and CPT π-π stacking **(Fig. 5)**. Both PEG_{45}-TetraCPT and PEG_{45}-OctaCPT presented improved therapeutic performances compared to spherical PEG_{45}-DiCPT **(Table 2),** like longer blood circulation, faster cell uptake and better drug release into the cytosol, making them good candidates for tumor drug delivery.

Another approach consisted in the conjugation of the drug directly to the polymeric nanoparticles after their formation by polymerization-induced self-assembly (PISA). PISA consists in the synthesis of block copolymers for which the block undergoing polymerization is insoluble in the reaction media, hence triggering the self-assembly *in situ*.[101,140] It has been shown that in the case of poly[oligo(ethyleneglycol)methacrylate]-*block*-[poly(styrene)-*co*-poly(vinyl benzaldehyde)] (POEGMA-*b*-P(ST-*co*-VBA)), the morphology of the aggregates was related to the degree of polymerization (DP_n) of the P(ST-*co*-VBA) block, forming the core of the nanoparticles. Transition towards elongated morphologies, like worms or rods, occurred with increasing reaction time. Reaction

with the aldehyde groups brought by the styrene units allowed then both crosslinking the core of the nanoassemblies and doxorubicin conjugation. However, this approach resulted in a drug loading of only 5 %, which remains a low value for chemical drug loading. These elongated morphologies revealed, however, decreased IC_{50} and increased cell uptake compared to spheres, but concerning drug release no significant differences were noted between the two structures **(Table 2)**. This method was further successfully applied to the conjugation of gadolinium complex Gd-DOTA to poly(glycidyl methacrylate)-based polymer, in order to build new worm-like MRI contrast agent with improved r_1 relaxivity comparatively to the spherical counterparts. And this was attributed to the larger core volume of worm-like micelles, hence slower rotational dynamics.[46]

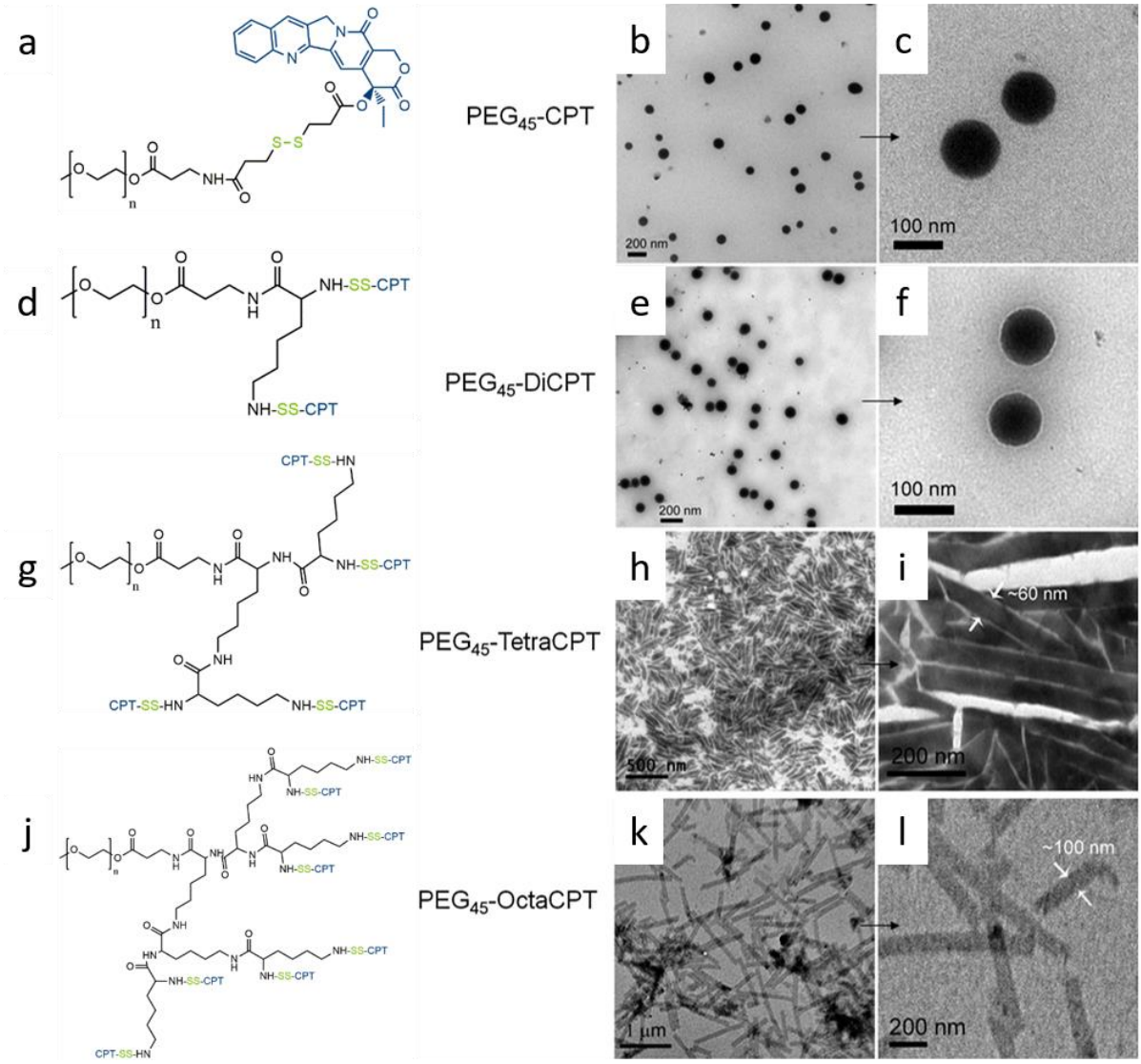

Fig. 5: Chemical structure and TEM images (various magnifications) of (a-c) PEG_{45}-CPT; (d-f) PEG_{45}-diCPT; (g-i) PEG_{45}-TetraCPT; (j-l) PEG_{45}-OctaCPT. Adapted with permission from [102].

4.2. Lipid-based conjugates

Nucleoside-lipid conjugates spontaneously forming wormlike micelles were revealed within the framework of extensive studies on the rich phase behavior of nucleolipids performed by Baglioni's and by Barthélémy's groups.[141–143] The first examples of "associative polynucleotides" were those of 1,2-dilauroyl (C12)-sn-glycero-3-phosphatidyl-adenosine and 1,2-dilauroyl (C12)-sn-glycero-3-phosphatidyl-uridine (DLPA and DLPU, respectively). DLPU self-assembled into long flexible cylindrical aggregates after solubilization in PBS (pH 7.5), with length growing with bioconjugate concentration. Replacing uridine by adenosine led to a more complex self-assembly pattern. The wormlike micelles evolved towards helical superstructures through micellar hierarchical aggregation upon aging. An explanation was found in the higher stacking properties of purine bases compared to pyrimidine ones, demonstrating that base-base interactions controlled the supramolecular structure.[48–50,135]

The pharmaceutical activity of DLPA was not investigated yet. However, these systems could open the way to the wormlike self-assembly of prodrugs of nucleoside analogues currently used in clinic against cancers and HIV-infections. Sandin *et al.* have synthesized a conjugate of clofarabine, a deoxyadenosine analogue active against leukemia, with 1,2-dilauroyl-sn-glycero-3-phosphatidyl *via* a phosphodiester bond.[144] The prodrug aggregates displayed a locally cylindrical structure. However, the stereochemistry of the polar head (at the SN2 carbon) was shown to induce an unexpected difference in wormlike micelle flexibility, resulting in different hierarchical associations of the primary micelles of the 2R and 2S diastereomers. The 2R-stereomer, sterically similar to phospholipids, yielded flexible wormlike micelles, which could wound around each other, forming helical superstructures. The 2S-stereomer gave rise to long stiff threads, often assembled through side-by-side interactions. This 2S derivative showed higher oral bioavailability and anti-tumor activity in vivo, which was tentatively explained by the diastereoselective self-assembly effect. Luan' group has designed amphiphilic prodrugs of cytarabine (Ara-C) for oral administration.[51–53] Cytarabine (1-(b-

D-arabinofuranosyl) cytosine) is a pyrimidine nucleoside analogue widely used against leukemia. Different lipid chains were linked to the NH2 group of Ara-C, namely oleic acid (OA, C18), lauric acid (LA, C12) and palmitic acid (PA, C16). Nanoprecipitation of prodrugs dissolved in methanol led to the formation of helical or twisted fibers, as shown by TEM. It has been suggested that OA-Ara fibers were formed by twisted multilayer ribbons. Of note, changes in the formulation process could induce modifications of the aggregate morphology. Although nanoprecipitation (bottom-up) followed by sonication, centrifugation and redispersion, on one hand, and dispersion of powder in water under sonication (top-down), on the other hand, both led to helical fibers, their length and rigidity differed. The top-down process yielded shorter straight helical fibers **(Fig. 6)**. Overall, the prodrugs significantly increased the oral bioavailability of Ara-C and enabled a sustained drug release in vivo.

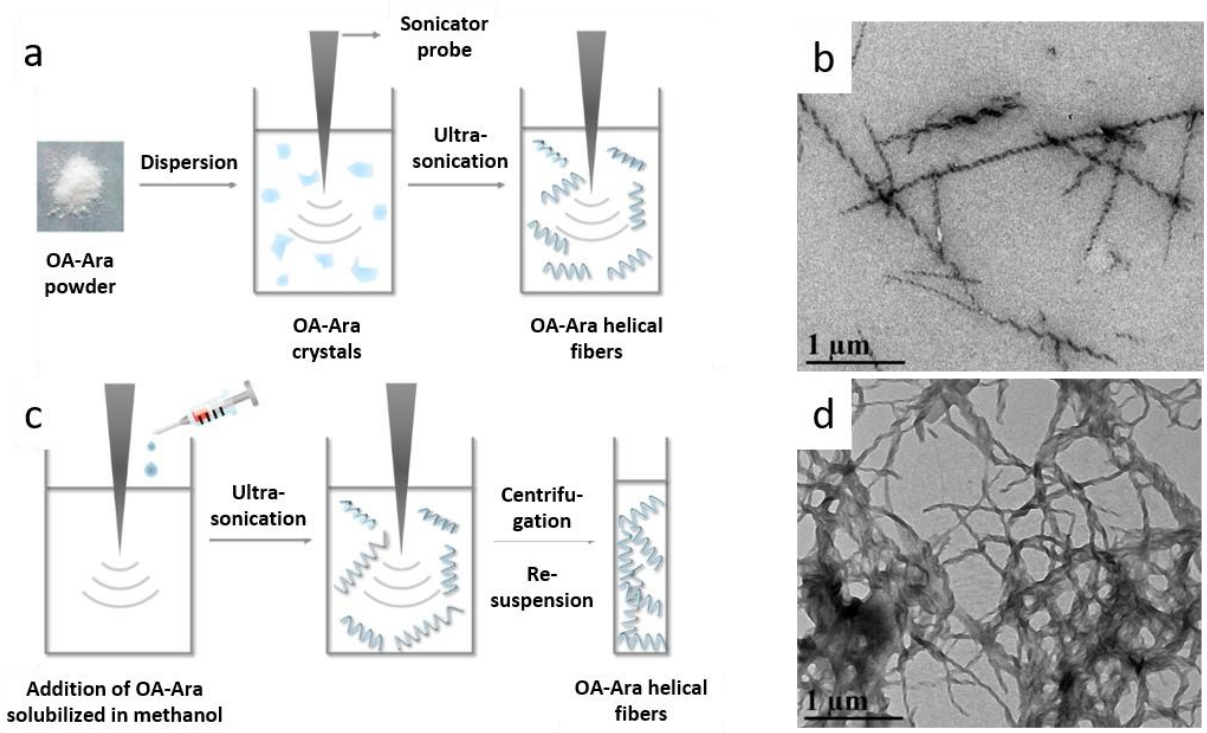

Fig. 6: Self-assembly of OA-Ara in aqueous media and TEM imaging. Spiral assemblies are prepared following (a; b) the top-down or (c; d) the bottom-up approaches. Adapted with permission from [51].

The so-called "squalenoylation" approach has been developed since 2006 by Couvreur's group. This method consists in the covalent coupling of various drugs to squalene, a natural triterpene precursor of the cholesterol biosynthesis.[145] Due to the dynamically folded conformation of

squalene, the resulting bioconjugates self-organized as spherical nanoparticles with improved pharmacological activity for the treatment of cancer [146,147], neurological disorders [148] as well as for pain alleviation [149] and even to control the paradoxal inflammation associated with COVID-19 infection [150]. Interestingly, concerning the shape of these squalene-based nanoassemblies, squalenoyl-doxorubicin (SQ-Dox) represents an exception, forming elongated cylinders refolding into loop-train rather than in spherical structures after simple nanoprecipitation into water. This unusual behavior originates from the strong π-π stacking propensity of DOX, enabling the formation of clusters of up to six DOX headgroups at the nanoparticles periphery. DOX stacking combined to hydrophobic squalene-squalene interactions drive the uniaxial growth of those nanoassemblies.[54] This original structure allowed decreasing the overall and cardiac toxicities, along with improved anticancer activity compared to free DOX. Still more interestingly, SQ-Dox was more potent than the two currently available liposomal formulations of doxorubicin, *ie*. Myocet and Caelyx.[136]

The influence of the length and nature of the terpenoid chain on the supramolecular organization of theses lipid-based bioconjugates has been investigated by Lepeltier *et al.* using Gemcitabine (Gem) as a model drug linked to polyisoprene chains built from 2 to 6 isoprene units.[108] Only conjugates with polyisoprene chains up to 5 units formed cylindrical assemblies. Bioconjugates comprising 2 to 4 isoprene units assembled into μms-long ribbons or nanotubes but appeared to precipitate in less than 1 hour. Oppositely, Gem-5-isoprene formed shorter but stable nanotubes. The stability and length of such assemblies resulted from a complex interplay between the solubility and diffusion coefficient of the bioconjugates and the presence of ethanol in the formulation media, altering the interfacial tension of the nanoassemblies. Interestingly, while squalenoyl-gemcitabine (Gem-SQ) structure differed from that of Gem-5-isoprene only by the position of two methyl groups on the hydrophobic chain, this molecule self-assembled into spheres with inverse hexagonal structure. This was explained by the difference in the rigidity of the squalene *versus* the isoprene chains. *In vitro* studies on MiaPaCa-2 and B16F10 cell lines demonstrated that Gem-Sq nanoparticles displayed higher cytotoxicity than Gem-5-isoprene nanotubes and this was correlated

with a slower cell uptake over 4 hours of the nanotubes. Those results were in agreement with the observations of Mitragotri and colleagues.[5,7]

4.3. Peptide-based conjugates

Inspired by the design of peptide amphiphiles, self-assembling peptide-drug conjugates, also called drug amphiphiles represent a new class of prodrugs built from a hydrophobic drug linked to a hydrophilic peptide through a cleavable linker. As a result, drug amphiphiles combine both the advantages of peptide-based nanocarriers, like a high degree of functionality, biodegradability and safety, and those of one-component nanomedicines, like an increased drug content in the 25-45 % range **(Table 4)**, and avoidance of the use of additional excipients.[151]

Similarly to peptide amphiphiles, drug amphiphiles easily self-assemble over hours after a single solubilization in water at physiological pH, hence avoiding the use of organic solvents whose residues can make the clinical development hazardous. However, the preparation of these nanomedicines requires more time. The self-assembling mechanism of drug amphiphiles relies on the π-π stacking properties of the drug headgroups, such as CPT or Ketoprofene (Ket), which drive the first steps of the self-assembly process by acting as anchors to initiate the building of the nanofibers core. Afterwards, the intermolecular H-bond between the peptide molecules would allow the β-sheet formation and the unidirectional growth.[55,152] Ket-L-VEVE drug amphiphile was used as a model to investigate this process in detail and to screen the external factors influencing the nanostructure, with the aim to establish a kind of a practical guide to design prodrugs self-assembling into particles with controlled morphologies. The pH of the nanofibers suspension was shown to modulate fibers diameters by acting on the ionization state of the conjugate. On another hand, the addition of H-binding inhibitor, such as urea, totally prevented the self-assembly. Of note, Ket-L-VEVE first assembled into nanorods undergoing ageing-induced transition towards nanofibers and multi-layered nanoribbons through end-to-end and fiber-to-fiber pathways. Twisting of the aggregates was a consequence of both the lateral stacking between fibers and the chirality of amino acids (**Fig. 7**).[55]

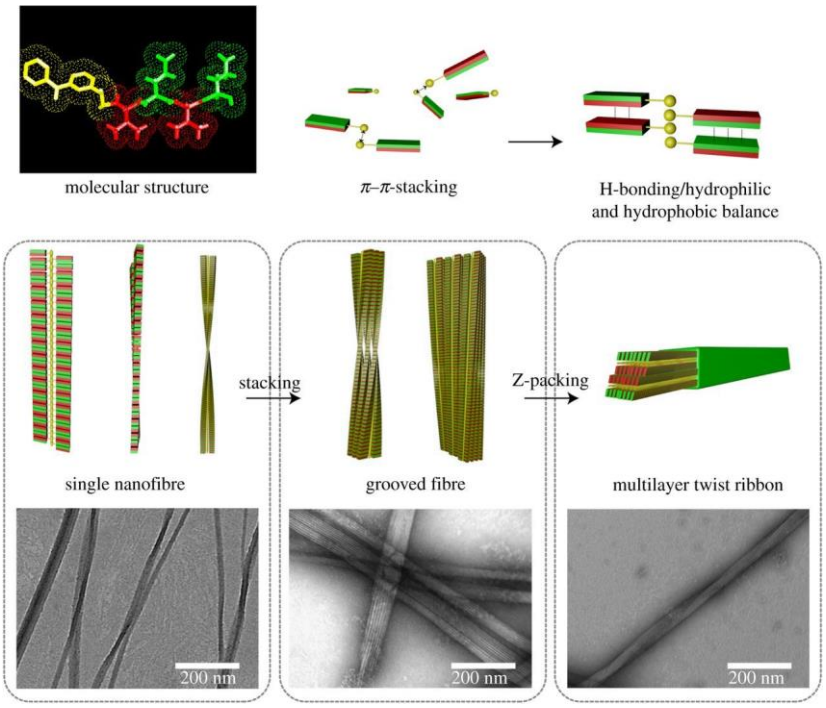

Fig. 7: The mechanism of Ket-L-VEVE self-assembly. Yellow represents the Ket moiety, red is for valine (V) and green for glutamic acid (E). Reprinted with permission from [55].

Cheetham *et al.* developed a drug amphiphile with high drug content for cancer treatment by using the β-sheet peptide VQIVYK, derived from the Tau protein, and conjugated to drug molecules through a 4-(pyridin-2-yl-disulfanyl)butyrate (buSS) linker, sensitive to the intracellular reducing agent glutathione (GSH). Conjugation with CPT led to CPT-buSS-Tau nanoaggregates with length and shape depending on the number of drug molecules conjugated to the peptide. Conjugates with 1 and 2 CPT molecules (mCPT-buSS-Tau and dCPT-buSS-Tau, respectively) formed nanofibers but dCPT-buSS-Tau displayed the most improved anticancer efficacy.[56] Starting from this conjugate, further investigations included comparison of different GSH-sensitive linkers [153], different hydrophilic moieties [137] or the use of a miktoarm star peptide, enabling the conjugation of different drugs (CPT and PTX) to the peptide bioconjugate, in order to overcome multi-drug resistance.[57] While all these molecular entities assembled into elongated shapes (nanofibers or nanotubes), the presence of β-sheet forming peptides, like Tau or Sup35, was mandatory to promote the formation of

nanofibers. However, the shape of these molecular assemblies was not the key parameter dictating the therapeutic efficacy, since surface chemistry and fast drug release were found to be much more influential.[137]

Another approach consisted in the *in situ* self-assembly of nanocarriers triggered by specific physiological parameters. As a proof of concept, Zhang *et al*. developed enzyme-responsive P18-PLGVRGRGD conjugate made of purpurin18 (P18) as the functional molecule (photosensitizer) with π-π stacking properties, PLGVRG as the enzyme-responsive sequence and RGD being the targeting ligand. The idea was to allow the diffusion of the hydrophilic bioconjugate into cancer cells. The linker peptide would then be cleaved by gelatinase, overexpressed in cancer cells. As a result, the drug hydrophobicity would increase, allowing the self-assembly as nanofibers which were able to increase the photoacoustic response for tumor detection, better than the controls not forming fibers. And an increased anti-cancer efficacy was also observed, consecutive to the slow activation of the drug release.[58] However, despite the promising results of this study, the authors of this review didn't find any further studies with a similar prodrug approach.

4.4. Supramolecular hydrogels

Under certain conditions, self-assembled drug-based conjugates can form supramolecular hydrogels, i.e., three-dimensional networks of physically cross-linked nanofibers, displaying viscoelasticity. Gelation occurs over hours and is usually induced by stimuli such as change in temperature[139], charge screening by electrolyte addition [62–65,138,154] or pH modification [155], enzymatic reaction etc.[155,156] The formulation of active substances into hydrogels allows their release up to several days at specific sites, making these systems particularly interesting for local drug delivery. So far, drug-based hydrogels have shown promising results in local cancer therapy and for anti-inflammatory treatments.

One of the first reported examples of prodrug-based hydrogels relied on an enzyme-sensitive drug amphiphile. In the early 2010's, Gao *et al.* coupled PTX *via* a succinic acid (SA) linker to a

peptide containing a phosphatase substrate sequence (NapFFKYp). The resulting PTX-SA-NapFFKYp was capable to form a gel upon overnight incubation with phosphatase. The enzyme converted this soluble precursor into a hydrogelator that self-assembled into nanofibers with a β-sheet-like structure. The obtained formulation preserved the anticancer activity of PTX, thanks to the slow release of the drug in physiological conditions without initial burst release (~ 3% in 24 h).[66]

Following the emergence of peptide amphiphiles (PAm), the Stupp group developed a hydrogelator PAm, consisting of a hydrophobic tail attached to a peptide sequence including a β -sheet forming sequence and charged residues (C16V2A2E2). The β -sheet forming sequence promoted the self-assembly of long nanofibers, while the addition of CaCl2 to screen electrostatic repulsion between nanofibers induced gelation at PAm concentration as low as 1 wt.%. The anti-inflammatory drugs nabumetone (Nb) [62] or dexamethasone (DEX) [154] were coupled to the end of the PAm molecule through a labile hydrazine linkage. Mixtures of Nb-PAm or DEX-PAm and PAm were also able to form nanofiber networks. Both drugs were found to be slowly released (~ 35% Nb released after 24 days and ~ 40% DEX released after 32 days) at physiological pH. The DEX hydrogel demonstrated cytoprotective and anti-inflammatory action in vitro and reduced the localized acute inflammatory response in mice.

Chakroun *et al.* have further investigated the mechanisms of release from hydrogels, using a peptide-based PTX conjugate, namely PTX-buSS-GGVVVRGDR, involving a β-sheet forming sequence (VVV) and a cell-penetrating peptide (RGDR) coupled to PTX *via* a disulfylbutyrate linker (buSS) and a spacer (GG). It was observed that the monomeric conjugate was released through the network swelling and disruption at the interface between the hydrogel and PBS, followed by nanofiber dissolution. Consequently, the release rate was found to depend on the network properties and on the stability of the nanofibers in PBS. The conjugate design could allow for the fine-tuning of its linear release rate. Decreasing the critical aggregation concentration (CAC) by adding an alkyl side chain (as a consequence of higher hydrophobicity) resulted in a slower drug release, while increasing the CAC by incorporating oppositely charged amino acids in the sequence favored an accelerated release (~ 1

and 7% over 1 month, respectively). The presence of the cell-penetrating peptide RGDR improved the tumor penetration and tumor growth inhibition in a U87 spheroid model.[157]

Inserting a peptide drug like tyroservatide (YSV) in the peptide sequence allowed further application of the supramolecular hydrogel approach to multidrug cancer therapy.[65] For example, the drug amphiphile CRB-FFE-YSV, obtained by coupling the small drug molecule chlorambucil (CRB) to the peptide sequence, was able to form a hydrogel *via* a heating- cooling process. The gel network conferred protection to the prodrug against enzymatic degradation, permitting high cellular uptake of the peptide-drug-conjugate released from the hydrogel. Owing to the synergy between CRB and YSV, the hydrogel displayed excellent antitumor activity in HepG2-tumor-bearing BALB/c nude mice. It was suggested that the decent biocompatibility of the hydrogel combined with a sustained and controllable drug release makes it interesting for local cancer treatment. Of course, this approach may find a limitation in the inability to reach potential metastasis anterior to the beginning of the treatment.[151]

Prodrugs based on SA and hydrophobic drugs capable of π-π stacking interactions (e.g., steroidal drugs) were also exploited to form hydrogels displaying a typical nanofiber structure. SA was successfully conjugated to DEX for ocular anti-inflammatory treatments [63,138,139] and to PTX for cancer therapy.[64] The low molecular weight of SA resulted in very impressive drug loadings, up to almost 90 wt.% in the case of PTX-SA (**Table 4**). Supramolecular hydrogels of DEX-SA or PTX-SA solubilized in PBS formed spontaneously after partial hydrolysis of the ester bond between the drug and SA for 24h (6.5 and 8.5 %, respectively).[63,64] Alternatively, gelation of DEX-SA could be triggered by the addition of divalent cations such as Ca^{2+}, owing to ionic coordination interactions between the divalent cations and the carboxylic acid groups.[138] Another drug for the management of intraocular inflammations, triamcinolone acetonide (TA), was conjugated to a glucosamine moiety (Glu) *via* a SA linkage.[139] Interestingly, TA-SA-Glu led to the formation in water of a thermoreversible hydrogel exhibiting a gel-sol transition at about 83°C. All these hydrogels had a low minimal gelation concentration, in the 0.25- 2 wt.% range, and exhibited an elastic behavior: their storage moduli (G') were greater than their loss moduli (G'') over the entire angular frequency ranges

investigated (0.1-10 or 0.1-100 rad.s-1). Increasing the hydrogelator concentration or the divalent cation concentration conferred improved mechanical strength to the gels and slowed down drug release. Furthermore, succinated prodrug hydrogelators formed thixotropic gels, becoming liquid when a shear rate was applied and reverting rapidly to the gel state at rest. In addition to the sustained and controlled release of the biologically active molecule, this approach is of particular interest for the design of injectable formulations for local treatment, but also for ocular administration. Indeed, such formulations could turn liquid when the patients blink and rapidly recover the gel state afterwards to progressively deliver the anti-inflammatory drug. Therefore, the DEX-SA and TA-SA-Glu hydrogels, exhibiting improved corneal retention and bioavailability with good intraocular biocompatibility, could be promising ocular drug delivery systems for hydrophobic DEX.

5. Pure nanodrugs

The design of pure nanodrugs represents a relevant approach for the delivery of drugs with self-aggregation properties and poor water solubility.[134] Based on these criteria, interest has been directed towards CPT and its derivatives. CPT is an antineoplastic agent constituted of five rings, one of which bearing a chiral center at position C_{20}, highly influencing the drug efficacy. However, CPT displays several limitations, such as a high toxicity and the sensitivity of the lactone ring to hydrolysis, turning rapidly after administration into the inactive carboxylate form.[158] To overcome those restrictions, numerous CPT derivatives have been synthesized but only few of them displayed self-assembling capabilities **(Fig. 8)**: CPT itself [67,68,159,160], 10-hydroxy camptothecin (HCPT) [47,69,70,105–107,160] and 7-ethyl-10-hydroxycamptohecin (SN-38) [71] bearing a hydroxyl function in C_{10} position to help stabilization in physiological medias [161], carboxylic camptothecin (CPT-COOH) [160] and camptothecin-20(*S*)-glycinate (CPT-NH_2) [70] for which the conjugation in the C_{20} position was expected to stabilize the lactone rings and to confer sustained release properties **(Fig. 8)**.[162,163]

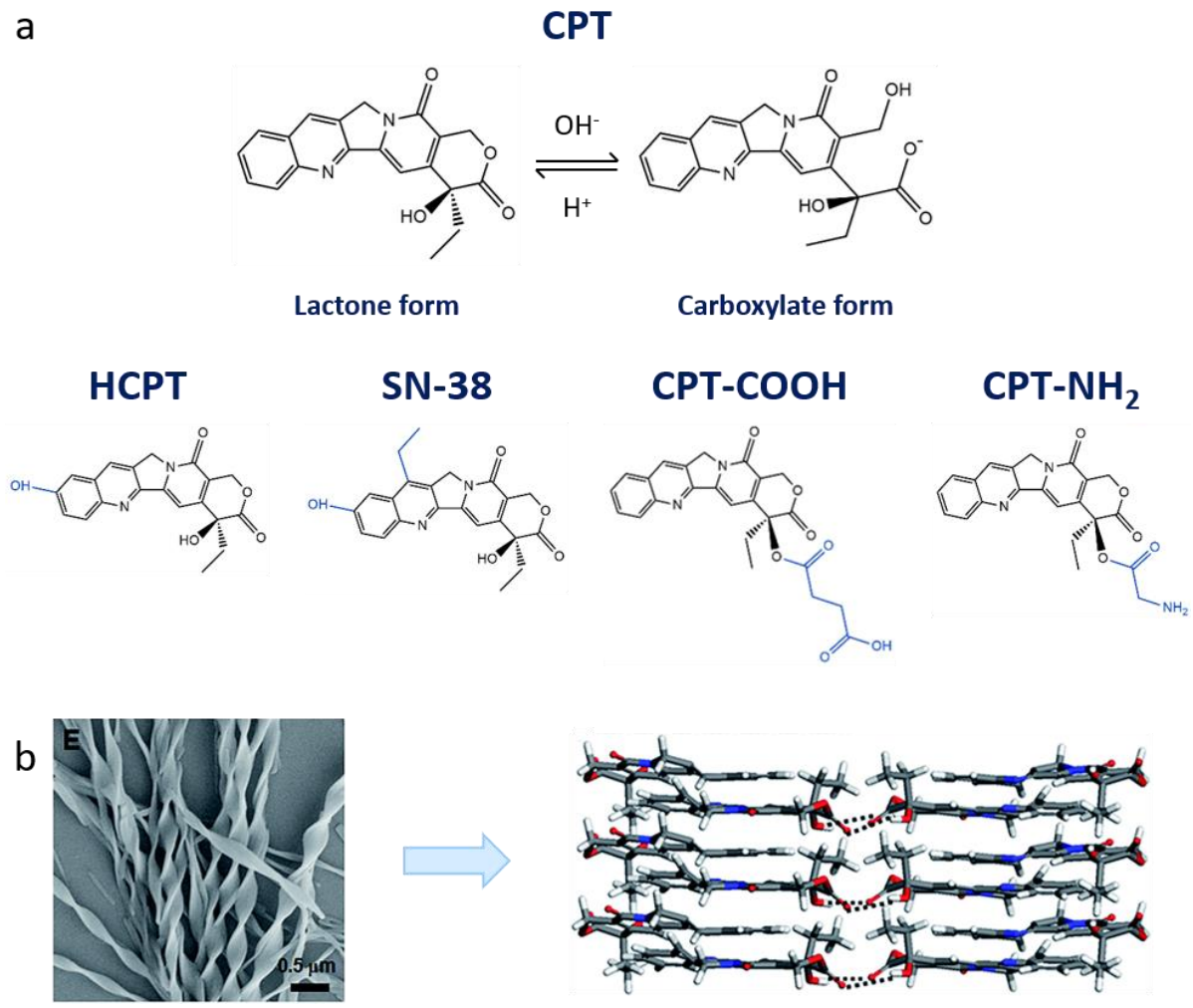

Fig. 8: CPT prodrugs. (a) Structure of CPT and its derivatives; (b). SEM image of CPT sample (3×10^{-4} mol L^{-1}) at room temperature and schematic illustration of molecules arrangement in CPT helical nanoribbons, dashed lines represent intermolecular H-bonds. Adapted with permission from [68].

CPT and analogues were found to self-assemble into aqueous media through a very easy process: after the solubilization of the drug in a solvent (usually dimethyl sulfoxide) and the addition of this solution to H_2O (under stirring or sonication), the helical nanoribbons formed. The planarity of CPT molecules combined to their π-π stacking and H-bonding properties likely favors the uniaxial growth of the fibers, forming edge-to-edge J-type stacks. Right-handed helicity has been reported, as a consequence of the presence of a chiral center in C_{20} position.[68,160] The stability of these nanostructures for several days suggests that the self-assembling enables the protection of the lactone ring. Nevertheless, Ma *et al.* took advantage of the sensitivity of this functional group to hydrolysis to trigger the pH-induced reversible assembly of CPT into nanofibers: raising the pH of a suspension of

CPT helical nanoribbons led to CPT solubilization, hence the disappearance of the nanostructures, when decreasing the pH back to 5 allowed the reversible formation of nanoribbons.[68] Additionally, the length of the CPT nanoribbons revealed to be tunable by adjusting the sonication time of the nano-suspension: longest sonication durations produced shorter lengths but without the destruction of the helical morphology. Interestingly, this observation allowed to maximize the therapeutic efficacy of those nanostructures, as it was shown that comparatively to the longer nanoribbons (several µm), short nanoribbons with ~ 1 µm length displayed an improved uptake by 4T1 cells, a higher cytotoxicity and a faster drug release.[159]

The self-assembly of CPT prodrugs was driven by the same stacking and H-bonding properties than the original drug, however with a loss of the helical conformation. Noteworthy, unlike CPT, the prodrug nanostructures revealed poor stability, as they started aggregating or sedimenting within minutes or hours. To overcome this limitation, different strategies were adopted. For example, the SN-38 CPT derivative was dimerized through various linkers (carbamate, ester or ether). However, this modification made the drug less planar, thus hindering the unidirectional growth and favoring the spherical morphology.[71]

Supramolecular elongated nanodrugs have been successfully used to encapsulate other small molecules for multidrug therapy. Mitragotri's group has proposed the first pure multidrug nanomedicine without using PEG or any other stabilizer. The design was as follows: CPT nanorods were coated with TTZ and loaded with DOX. Those three drugs were distributed into different cell compartments (late endosomes, recycled in plasma membrane, or in nucleus for CPT, TTZ and DOX, respectively), hence allowing cytoplasmic targeting and synergistic anticancer efficacy against BT-474 breast cancer cells.[67] More recently, combinations of a drug with a photosensitizer were also proposed such as HCPT/chlorin e6 (Ce6) [69] or PTX/ di-iodinated borondipyrromethene [164] for dual chemo-photodynamic therapy purposes. Such formulations revealed superior anticancer activity comparatively to the corresponding monotherapies, allowing complete tumor growth inhibition *in vivo*, while reducing side effects.

6. Toxicity of elongated nanomedicines

As discussed in the above sections, one of the main features of elongated nanoparticles is their long-circulating properties. As a consequence, it is legitimate to wonder about their possible long-term toxicity after *in vivo* administration.

Among the available literature, cancer remains the most studied pathology. And anti-cancer treatments are generally administered by multiple intravenous injections, the overall toxicity being usually detected through body weight variations. Christian *et al.* demonstrated that A549 tumor-bearing Nrc nude mice treated with PTX-loaded filomicelles at the maximum tolerated dose didn't reveal significant body weight difference over the 21-days of experiment, compared to other groups treated with either PBS saline, free PTX or empty filomicelles, thus indicating the absence of impact on the overall health.[10] Other studies demonstrating similar findings were obtained with other types of carriers, such as HCPT-loaded PEG nanorods [165], CPT-loaded peptide amphiphiles [43], SQ-Dox drug-lipid conjugate [136], Dox-peptide conjugate-based nanofibers[60] or MTX/HCPT/PTX or icaritin and derivatives nanocrystals [102,166]. In addition, besides improved tumor accumulation, elongated nanocarriers also tend to accumulate in the organs of the reticuloendothelial system (RES).[60,102,106,136,165] Wen *et al.* used Ce6-loaded HCPT nanorods as a new photodynamic therapy and histological examination of vital organ tissue (lung, heart, spleen, kidney and liver) didn't show any lesion for treated animals, even after laser irradiation, confirming the safety of those nanocarriers.[69] More recently, tissue examination of HepG2 BALB/c mice treated with CRB-FFE-YSV nanofiber-based hydrogel didn't either reveal noticeable damage to major organs.[65]

By comparing studies dealing with carbon nanotubes (CNT) *in vivo,* Kinnear *et al.* have, however, pointed out the dependence of the toxicity of nanomedicines on the administration route. [167] While peritoneal instillation of long CNT in mice displayed granulomatous inflammation and lesion similar to abestos-like pathology [168], Schipper *et al*. demonstrated that, upon intravenous administration to nude mice, Peg-functionalized single-walled CNT persisted within liver and spleen

macrophages over four months without significant toxicity.[169] Alternatively to intravenous injection, Cinar *et al.* administered Dox-loaded peptide amphiphile nanofibers *via* single subcutaneous injection to BALB/c mice grafted with 4T1 breast cancer tumor. Interestingly, they didn't observe any weight loss for nanofibers-treated animals, as opposed to a slight weight loss for free Dox and control groups. Furthermore, tissue morphology of liver, kidney and spleen of treated animals were similar to that of control untreated animals. Hence, no toxicity was attributable to the nanofibers.[132] Treatments administered by single or repeated intra-tumoral injections [60,164], or by oral route [170] didn't display different toxicity patterns, too. To corroborate histological observations, Liu *et al.* investigated potential hepatotoxicity. No significant change in serum levels of alanine aminotransferase, serum aspartate aminotransferase (AST), creatine or blood urea nitrogen (BUN) levels were evidenced between nanofibers-treated and untreated animal.[170] Altogether, these studies didn't show any toxicity of the elongated nanomedicine whatever the administration route.

Furthermore, elongated nanomedicine were successfully applied to the treatment of other pathologies. For example, Dex-PAm was successfully employed as an anti-inflammatory nanomedicine. Inflammation was triggered by the injection of polystyrene particles to hairless SKH1/E mice. Single subcutaneous administration of Dex-PAm nanofibers resulted in an anti-inflammatory action localized in the area of injection, without any visible fibrosis or inflammation in the treated tissues. [154] Mansukhani *et al.* developed peptide amphiphile nanofibers based on apolipoprotein A1-derived targeting peptide and liver X receptor agonist GW3965 (ApoA1-LXR PA) to target atherosclerotic lesions. After repeated intravenous injections in LDLR-KO mice fed with high fat diet, AST levels of animal treated were similar to PBS saline-treated group after 8-week treatment, indicating no hepatotoxicity.[171]

Noteworthy is that if most of the published studies investigated the toxicity of self-assembled cylindrical nanomedicines comparatively to free drugs, empty nanocarriers and PBS saline as controls, very few tackle the issue of shape-related toxicity. This results from the difficulty to form spheres and cylinders of similar composition. However, Discher's group succeeded in preparing both spherical and cylindrical polymeric PTX-loaded micelles of same composition.[9] Interestingly, the body weight

loss of A549-tumor bearing Nrc nude mice remained comparable in animals treated with spherical or cylindrical micelles. Consequently, no shape-dependent toxicity could be established.[10] In another study, HeLa BALB/c mice were administered either with spherical or cylindrical MTX-PEG-CPT nanoparticles. While animals treated with free drugs or spherical nanoparticles suffered of a significant body weight loss, animals administered with saline solution or nanorods maintained their weight throughout the 14-days experiment, confirming the safety of cylindrical nanocarriers.[107] Nevertheless, conflicting results were found in other investigations. Indeed, PEGylated HCPT nanorods displayed significant toxicity when compared to nanospheres of same composition after intravenous administration to 4T1 tumor-bearing BALB/c mice. This was evidenced by an alteration of the overall health of the treated animals (*ie*. durable weight loss and decreased activity) associated to the formation of microganula in the liver. Significantly lower levels of white blood cells 7 days post injection for animals treated with nanorods compared to the control group and animals treated with nanospheres evidenced hematological toxicity. Additionally, low levels of BUN, albumin and total protein up to 30 days post injection, were associated to long-term toxicity, thus confirming a shape-induced toxicity of nanorods over nanospheres.[106]

If trends seem to emerge concerning the safety of cylindrical, self-assembled, biodegradable nanomedicines compared to free drugs, independently of the administration route, the results are much more contrasted in terms of shape-related toxicity. Indeed, the limited number of toxicity studies currently available do not allow to clearly draw valid conclusions. This issues will need to raise more attention in the future.

7. Conclusion

Important progresses have been realized over the last years in the comprehension of the driving forces triggering the formation of cylindrical nanoparticles (filomicelles, worm-like or rod-like nanoparticles, nanofibers etc…). The self-assembling mechanism and supramolecular organization are key parameters to optimize the therapeutic efficacy of nanomedicines. Their understanding has

allowed to formulate drug delivery devices using a wide range of biocompatible materials, from simple lipids or diblock polymers to more complex materials functionalized with targeting ligands, stimuli-responsive moieties and loading several drugs and/or dyes for theranostic applications. The viscoelasticity of worm-like particles has also successfully been exploited to design hydrogels suitable for local delivery.

All the described approaches have, however, both advantages and limitations, making difficult the task of designing an ideal cylindrical nanocarrier. Bioconjugates and pure nanodrug approaches are probably more promising than what we have called the physical encapsulation, in terms of drug loading capacity and avoidance of burst release after administration. Indeed, using a limited amount of carrier material may help to avoid potential toxicological issues. However, the synthesis of some bioconjugates may require sophisticated chemistry, while the nanodrug design may also necessitate the addition of PEG to be stable in biological environments. Among the various drug conjugates, polymer-drug conjugates are probably among the easiest to be designed and functionalized. Similarly to lipid-conjugates, their formulation is generally rapid but requires the use of organic solvent that will need to be removed. Peptide-drug conjugates circumvent this drawback, as they simply assemble after dispersion in water. But this process is time-consuming as it needs hours to days to equilibrate. Furthermore, most of these strategies apply to a limited number of drug molecules, as they often rely on π-π stacking properties to form the elongated nanostructures. Nevertheless, despite the difficulty to design the ideal cylindrical drug delivery system, all reports tackling the comparison between spherical and cylindrical nanovectors agreed on the therapeutic benefits brought by the latter in preclinical *in vitro* or *in vivo* experiments. However, none of the elongated nanostructures discussed in this review have already reached a clinical stage of development, likely because the reproducibility of the obtained elongated nanostructures (*ie.* length and thickness) still remains unable to meet the usual pharmaceutical requirements. But the unique pre-clinical data of these nanocarriers as detailed in the present review should encourage further investigations concerning their scaling-up and reproducilility.

References

[1] H.H. Gustafson, D. Holt-Casper, D.W. Grainger, H. Ghandehari, Nanoparticle uptake: The phagocyte problem, Nano Today. 10 (2015) 487–510. https://doi.org/10.1016/j.nantod.2015.06.006.

[2] M. Lundqvist, J. Stigler, G. Elia, I. Lynch, T. Cedervall, K.A. Dawson, Nanoparticle size and surface properties determine the protein corona with possible implications for biological impacts, Proc. Natl. Acad. Sci. 105 (2008) 14265–14270. https://doi.org/10.1073/pnas.0805135105.

[3] A.L. Klibanov, K. Maruyama, V.P. Torchilin, L. Huang, Amphipathic polyethyleneglycols effectively prolong the circulation time of liposomes, FEBS Lett. 268 (1990) 235–237. https://doi.org/10.1016/0014-5793(90)81016-H.

[4] R. Gref, Y. Minamitake, M. Peracchia, V. Trubetskoy, V. Torchilin, R. Langer, Biodegradable long-circulating polymeric nanospheres, Science. 263 (1994) 1600–1603. https://doi.org/10.1126/science.8128245.

[5] J.A. Champion, S. Mitragotri, Role of target geometry in phagocytosis, Proc. Natl. Acad. Sci. 103 (2006) 4930–4934. https://doi.org/10.1073/pnas.0600997103.

[6] G. Sharma, D.T. Valenta, Y. Altman, S. Harvey, H. Xie, S. Mitragotri, J.W. Smith, Polymer particle shape independently influences binding and internalization by macrophages, J. Controlled Release. 147 (2010) 408–412. https://doi.org/10.1016/j.jconrel.2010.07.116.

[7] J.A. Champion, S. Mitragotri, Shape Induced Inhibition of Phagocytosis of Polymer Particles, Pharm. Res. 26 (2009) 244–249. https://doi.org/10.1007/s11095-008-9626-z.

[8] Y. Geng, P. Dalhaimer, S. Cai, R. Tsai, M. Tewari, T. Minko, D.E. Discher, Shape effects of filaments versus spherical particles in flow and drug delivery, Nat. Nanotechnol. 2 (2007) 249–255. https://doi.org/10.1038/nnano.2007.70.

[9] S. Cai, K. Vijayan, D. Cheng, E.M. Lima, D.E. Discher, Micelles of Different Morphologies—Advantages of Worm-like Filomicelles of PEO-PCL in Paclitaxel Delivery, Pharm. Res. 24 (2007) 2099–2109. https://doi.org/10.1007/s11095-007-9335-z.

[10] D.A. Christian, S. Cai, O.B. Garbuzenko, T. Harada, A.L. Zajac, T. Minko, D.E. Discher, Flexible Filaments for in Vivo Imaging and Delivery: Persistent Circulation of Filomicelles Opens the Dosage Window for Sustained Tumor Shrinkage, Mol. Pharm. 6 (2009) 1343–1352. https://doi.org/10.1021/mp900022m.

[11] Z. Zhao, A. Ukidve, V. Krishnan, S. Mitragotri, Effect of physicochemical and surface properties on in vivo fate of drug nanocarriers, Adv. Drug Deliv. Rev. 143 (2019) 3–21. https://doi.org/10.1016/j.addr.2019.01.002.

[12] S. Venkataraman, J.L. Hedrick, Z.Y. Ong, C. Yang, P.L.R. Ee, P.T. Hammond, Y.Y. Yang, The effects of polymeric nanostructure shape on drug delivery, Adv. Drug Deliv. Rev. 63 (2011) 1228–1246. https://doi.org/10.1016/j.addr.2011.06.016.

[13] P. Decuzzi, R. Pasqualini, W. Arap, M. Ferrari, Intravascular Delivery of Particulate Systems: Does Geometry Really Matter?, Pharm. Res. 26 (2009) 235–243. https://doi.org/10.1007/s11095-008-9697-x.

[14] J.D. Pillai, S.S. Dunn, M.E. Napier, J.M. DeSimone, Novel platforms for vascular carriers with controlled geometry, IUBMB Life. 63 (2011) 596–606. https://doi.org/10.1002/iub.497.

[15] E.A. Simone, T.D. Dziubla, V.R. Muzykantov, Polymeric carriers: role of geometry in drug delivery, Expert Opin. Drug Deliv. 5 (2008) 1283–1300. https://doi.org/10.1517/17425240802567846.

[16] N.P. Truong, M.R. Whittaker, C.W. Mak, T.P. Davis, The importance of nanoparticle shape in cancer drug delivery, Expert Opin. Drug Deliv. 12 (2015) 129–142. https://doi.org/10.1517/17425247.2014.950564.

[17] T.J. Merkel, K.P. Herlihy, J. Nunes, R.M. Orgel, J.P. Rolland, J.M. DeSimone, Scalable, Shape-Specific, Top-Down Fabrication Methods for the Synthesis of Engineered Colloidal Particles, Langmuir. 26 (2010) 13086–13096. https://doi.org/10.1021/la903890h.

[18] J.L. Perry, K.P. Herlihy, M.E. Napier, J.M. DeSimone, PRINT: A Novel Platform Toward Shape and Size Specific Nanoparticle Theranostics, Acc. Chem. Res. 44 (2011) 990–998. https://doi.org/10.1021/ar2000315.

[19] K.S. Chu, W. Hasan, S. Rawal, M.D. Walsh, E.M. Enlow, J.C. Luft, A.S. Bridges, J.L. Kuijer, M.E. Napier, W.C. Zamboni, J.M. DeSimone, Plasma, tumor and tissue pharmacokinetics of Docetaxel delivered *via* nanoparticles of different sizes and shapes in mice bearing SKOV-3 human ovarian carcinoma xenograft, Nanomedicine Nanotechnol. Biol. Med. 9 (2013) 686–693. https://doi.org/10.1016/j.nano.2012.11.008.

[20] R.A. Petros, P.A. Ropp, J.M. DeSimone, Reductively Labile PRINT Particles for the Delivery of Doxorubicin to HeLa Cells, J. Am. Chem. Soc. 130 (2008) 5008–5009. https://doi.org/10.1021/ja801436j.

[21] L.P.D. Ratcliffe, M.J. Derry, A. Ianiro, R. Tuinier, S.P. Armes, A Single Thermoresponsive Diblock Copolymer Can Form Spheres, Worms or Vesicles in Aqueous Solution, Angew. Chem. Int. Ed. 58 (2019) 18964–18970. https://doi.org/10.1002/anie.201909124.

[22] Y. Geng, F. Ahmed, N. Bhasin, D.E. Discher, Visualizing Worm Micelle Dynamics and Phase Transitions of a Charged Diblock Copolymer in Water, J. Phys. Chem. B. 109 (2005) 3772–3779. https://doi.org/10.1021/jp0459559.

[23] K. Jelonek, S. Li, B. Kaczmarczyk, A. Marcinkowski, A. Orchel, M. Musiał-Kulik, J. Kasperczyk, Multidrug PLA-PEG filomicelles for concurrent delivery of anticancer drugs—The influence of drug-drug and drug-polymer interactions on drug loading and release properties, Int. J. Pharm. 510 (2016) 365–374. https://doi.org/10.1016/j.ijpharm.2016.06.051.

[24] K. Jelonek, S. Li, X. Wu, J. Kasperczyk, A. Marcinkowski, Self-assembled filomicelles prepared from polylactide/poly(ethylene glycol) block copolymers for anticancer drug delivery, Int. J. Pharm. 485 (2015) 357–364. https://doi.org/10.1016/j.ijpharm.2015.03.032.

[25] P.R. Nair, S. Karthick, K.R. Spinler, M.R. Vakili, A. Lavasanifar, D.E. Discher, Filomicelles from aromatic diblock copolymers increase paclitaxel-induced tumor cell death and aneuploidy compared with aliphatic copolymers, Nanomed. 11 (2016) 1551–1569. https://doi.org/10.2217/nnm-2016-0007.

[26] C.A. Dreiss, Wormlike micelles: where do we stand? Recent developments, linear rheology and scattering techniques, Soft Matter. 3 (2007) 956–970. https://doi.org/10.1039/b705775j.

[27] X. Sun, X. Liu, C. Li, Y. Wang, L. Liu, F. Su, S. Li, Self-assembled micelles prepared from poly(ε-caprolactone)-poly(ethylene glycol) and poly(ε-caprolactone/glycolide)-poly(ethylene glycol) block copolymers for sustained drug delivery, J. Appl. Polym. Sci. 135 (2018) 45732. https://doi.org/10.1002/app.45732.

[28] F. Gharebaghi, N. Dalali, E. Ahmadi, H. Danafar, Preparation of wormlike polymeric nanoparticles coated with silica for delivery of methotrexate and evaluation of anticancer activity against MCF7 cells, J. Biomater. Appl. 31 (2017) 1305–1316. https://doi.org/10.1177/0885328217698063.

[29] P. Zhao, L. Liu, X. Feng, C. Wang, X. Shuai, Y. Chen, Molecular Nanoworm with PCL Core and PEO Shell as a Non-spherical Carrier for Drug Delivery, Macromol. Rapid Commun. 33 (2012) 1351–1355. https://doi.org/10.1002/marc.201200172.

[30] X. He, H. Yu, X. Bao, H. Cao, Q. Yin, Z. Zhang, Y. Li, pH-Responsive Wormlike Micelles with Sequential Metastasis Targeting Inhibit Lung Metastasis of Breast Cancer, Adv. Healthc. Mater. 5 (2016) 439–448. https://doi.org/10.1002/adhm.201500626.

[31] K. Jelonek, S. Li, J. Kasperczyk, X. Wu, A. Orchel, Effect of polymer degradation on prolonged release of paclitaxel from filomicelles of polylactide/poly(ethylene glycol) block copolymers, Mater. Sci. Eng. C. 75 (2017) 918–925. https://doi.org/10.1016/j.msec.2017.03.006.

[32] K. Jelonek, J. Kasperczyk, S. Li, T.H.N. Nguyen, A. Orchel, E. Chodurek, P. Paduszyński, M. Jaworska-Kik, E. Chrobak, E. Bębenek, S. Boryczka, M. Jarosz-Biej, R. Smolarczyk, A. Foryś, Bioresorbable filomicelles for targeted delivery of betulin derivative – In vitro study, Int. J. Pharm. 557 (2019) 43–52. https://doi.org/10.1016/j.ijpharm.2018.12.033.

[33] X. Yang, J.J. Grailer, I.J. Rowland, A. Javadi, S.A. Hurley, D.A. Steeber, S. Gong, Multifunctional SPIO/DOX-loaded wormlike polymer vesicles for cancer therapy and MR imaging, Biomaterials. 31 (2010) 9065–9073. https://doi.org/10.1016/j.biomaterials.2010.08.039.

[34] K. Sarkar, S.R. Krishna Meka, G. Madras, K. Chatterjee, A self-assembling polycationic nanocarrier that exhibits exceptional gene transfection efficiency, RSC Adv. 5 (2015) 91619–91632. https://doi.org/10.1039/C5RA14829D.

[35] J.-M. Williford, M.M. Archang, I. Minn, Y. Ren, M. Wo, J. Vandermark, P.B. Fisher, M.G. Pomper, H.-Q. Mao, Critical Length of PEG Grafts on lPEI/DNA Nanoparticles for Efficient in Vivo Delivery, ACS Biomater. Sci. Eng. 2 (2016) 567–578. https://doi.org/10.1021/acsbiomaterials.5b00551.

[36] X. Wan, Y. Min, H. Bludau, A. Keith, S.S. Sheiko, R. Jordan, A.Z. Wang, M. Sokolsky-Papkov, A.V. Kabanov, Drug Combination Synergy in Worm-like Polymeric Micelles Improves Treatment Outcome for Small Cell and Non-Small Cell Lung Cancer, ACS Nano. 12 (2018) 2426–2439. https://doi.org/10.1021/acsnano.7b07878.

[37] S. Yi, S.D. Allen, Y.-G. Liu, B.Z. Ouyang, X. Li, P. Augsornworawat, E.B. Thorp, E.A. Scott, Tailoring Nanostructure Morphology for Enhanced Targeting of Dendritic Cells in Atherosclerosis, ACS Nano. 10 (2016) 11290–11303. https://doi.org/10.1021/acsnano.6b06451.

[38] T.H. Kim, C.W. Mount, B.W. Dulken, J. Ramos, C.J. Fu, H.A. Khant, W. Chiu, W.R. Gombotz, S.H. Pun, Filamentous, Mixed Micelles of Triblock Copolymers Enhance Tumor Localization of Indocyanine Green in a Murine Xenograft Model, Mol. Pharm. 9 (2012) 135–143. https://doi.org/10.1021/mp200381c.

[39] H. Li, H. Liu, T. Nie, Y. Chen, Z. Wang, H. Huang, L. Liu, Y. Chen, Molecular bottlebrush as a unimolecular vehicle with tunable shape for photothermal cancer therapy, Biomaterials. 178 (2018) 620–629. https://doi.org/10.1016/j.biomaterials.2018.03.032.

[40] S. Aluri, M.K. Pastuszka, A.S. Moses, J.A. MacKay, Elastin-Like Peptide Amphiphiles Form Nanofibers with Tunable Length, Biomacromolecules. 13 (2012) 2645–2654. https://doi.org/10.1021/bm300472y.

[41] P. Zhang, A.G. Cheetham, Y. Lin, H. Cui, Self-Assembled Tat Nanofibers as Effective Drug Carrier and Transporter, ACS Nano. 7 (2013) 5965–5977. https://doi.org/10.1021/nn401667z.

[42] M.J. Webber, C.J. Newcomb, R. Bitton, S.I. Stupp, Switching of self-assembly in a peptide nanostructure with a specific enzyme, Soft Matter. 7 (2011) 9665. https://doi.org/10.1039/c1sm05610g.

[43] S. Soukasene, D.J. Toft, T.J. Moyer, H. Lu, H.-K. Lee, S.M. Standley, V.L. Cryns, S.I. Stupp, Antitumor Activity of Peptide Amphiphile Nanofiber-Encapsulated Camptothecin, ACS Nano. 5 (2011) 9113–9121. https://doi.org/10.1021/nn203343z.

[44] M.M. So, N.A. Mansukhani, E.B. Peters, M.S. Albaghdadi, Z. Wang, C.M. Rubert Pérez, M.R. Kibbe, S.I. Stupp, Peptide Amphiphile Nanostructures for Targeting of Atherosclerotic Plaque and Drug Delivery, Adv. Biosyst. 2 (2018) 1700123. https://doi.org/10.1002/adbi.201700123.

[45] J.-K. Kim, J. Anderson, H.-W. Jun, M.A. Repka, S. Jo, Self-Assembling Peptide Amphiphile-Based Nanofiber Gel for Bioresponsive Cisplatin Delivery, Mol. Pharm. 6 (2009) 978–985. https://doi.org/10.1021/mp900009n.

[46] L. Esser, N.P. Truong, B. Karagoz, B.A. Moffat, C. Boyer, J.F. Quinn, M.R. Whittaker, T.P. Davis, Gadolinium-functionalized nanoparticles for application as magnetic resonance imaging contrast agents *via* polymerization-induced self-assembly, Polym. Chem. 7 (2016) 7325–7337. https://doi.org/10.1039/C6PY01797E.

[47] M. Zhou, X. Zhang, Y. Yang, Z. Liu, B. Tian, J. Jie, X. Zhang, Carrier-free functionalized multidrug nanorods for synergistic cancer therapy, Biomaterials. 34 (2013) 8960–8967. https://doi.org/10.1016/j.biomaterials.2013.07.080.

[48] F. Baldelli Bombelli, D. Berti, U. Keiderling, P. Baglioni, Living polynucleotides formed by the spontaneous aggregation of dilauroylphosphonucleosides, Appl. Phys. Mater. Sci. Process. 74 (2002) s1270–s1273. https://doi.org/10.1007/s003390101217.

[49] F.B. Bombelli, D. Berti, F. Pini, U. Keiderling, P. Baglioni, Flexibility of Dilauroyl-Phosphatidyl-Nucleoside Wormlike Micelles in Aqueous Solutions, J. Phys. Chem. B. 108 (2004) 16427–16434. https://doi.org/10.1021/jp047816x.

[50] F.B. Bombelli, D. Berti, M. Almgren, G. Karlsson, P. Baglioni, Light Scattering and Cryo-Transmission Electron Microscopy Investigation of the Self-Assembling Behavior of Di-C 12

P-Nucleosides in Solution, J. Phys. Chem. B. 110 (2006) 17627–17637. https://doi.org/10.1021/jp060594d.

[51] J. Liu, N. Ma, D. Zhao, Z. Li, Y. Luan, Spiral assembly of amphiphilic cytarabine prodrug assisted by probe sonication: Enhanced therapy index for leukemia, Colloids Surf. B Biointerfaces. 136 (2015) 918–927. https://doi.org/10.1016/j.colsurfb.2015.10.034.

[52] J. Liu, J. Liu, D. Zhao, N. Ma, Y. Luan, Highly enhanced leukemia therapy and oral bioavailability from a novel amphiphilic prodrug of cytarabine, RSC Adv. 6 (2016) 35991–35999. https://doi.org/10.1039/C6RA02051H.

[53] J. Zhang, D. Zhang, X. Hu, R. Liu, Z. Li, Y. Luan, Rational design of a new cytarabine-based prodrug for highly efficient oral delivery of cytarabine, RSC Adv. 8 (2018) 13103–13111. https://doi.org/10.1039/C8RA01225C.

[54] J. Mougin, S.O. Yesylevskyy, C. Bourgaux, D. Chapron, J.-P. Michel, F. Dosio, B. Stella, C. Ramseyer, P. Couvreur, Stacking as a Key Property for Creating Nanoparticles with Tunable Shape: The Case of Squalenoyl-Doxorubicin, ACS Nano. 13 (2019) 12870–12879. https://doi.org/10.1021/acsnano.9b05303.

[55] Q. Fan, Y. Ji, J. Wang, L. Wu, W. Li, R. Chen, Z. Chen, Self-assembly behaviours of peptide–drug conjugates: influence of multiple factors on aggregate morphology and potential self-assembly mechanism, R. Soc. Open Sci. 5 (2018) 172040. https://doi.org/10.1098/rsos.172040.

[56] A.G. Cheetham, P. Zhang, Y. Lin, L.L. Lock, H. Cui, Supramolecular Nanostructures Formed by Anticancer Drug Assembly, J. Am. Chem. Soc. 135 (2013) 2907–2910. https://doi.org/10.1021/ja3115983.

[57] A.G. Cheetham, P. Zhang, Y.-A. Lin, R. Lin, H. Cui, Synthesis and self-assembly of a mikto-arm star dual drug amphiphile containing both paclitaxel and camptothecin, J Mater Chem B. 2 (2014) 7316–7326. https://doi.org/10.1039/C4TB01084A.

[58] D. Zhang, G.-B. Qi, Y.-X. Zhao, S.-L. Qiao, C. Yang, H. Wang, In Situ Formation of Nanofibers from Purpurin18-Peptide Conjugates and the Assembly Induced Retention Effect in Tumor Sites, Adv. Mater. 27 (2015) 6125–6130. https://doi.org/10.1002/adma.201502598.

[59] M. Yang, D. Xu, L. Jiang, L. Zhang, D. Dustin, R. Lund, L. Liu, H. Dong, Filamentous supramolecular peptide–drug conjugates as highly efficient drug delivery vehicles, Chem Commun. 50 (2014) 4827–4830. https://doi.org/10.1039/C4CC01568A.

[60] Y. Ji, Y. Xiao, L. Xu, J. He, C. Qian, W. Li, L. Wu, R. Chen, J. Wang, R. Hu, X. Zhang, Z. Gu, Z. Chen, Drug-Bearing Supramolecular MMP Inhibitor Nanofibers for Inhibition of Metastasis and Growth of Liver Cancer, Adv. Sci. 5 (2018) 1700867. https://doi.org/10.1002/advs.201700867.

[61] R. Lin, A.G. Cheetham, P. Zhang, Y. Lin, H. Cui, Supramolecular filaments containing a fixed 41% paclitaxel loading, Chem. Commun. 49 (2013) 4968. https://doi.org/10.1039/c3cc41896k.

[62] J.B. Matson, S.I. Stupp, Drug release from hydrazone-containing peptide amphiphiles, Chem. Commun. 47 (2011) 7962. https://doi.org/10.1039/c1cc12570b.

[63] Z. Zhang, J. Yu, Y. Zhou, R. Zhang, Q. Song, L. Lei, X. Li, Supramolecular nanofibers of dexamethasone derivatives to form hydrogel for topical ocular drug delivery, Colloids Surf. B Biointerfaces. 164 (2018) 436–443. https://doi.org/10.1016/j.colsurfb.2018.01.051.

[64] Q. Song, R. Zhang, L. Lei, X. Li, Self-Assembly of Succinated Paclitaxel into Supramolecular Hydrogel for Local Cancer Chemotherapy, J. Biomed. Nanotechnol. 14 (2018) 1471–1476. https://doi.org/10.1166/jbn.2018.2595.

[65] L. Yang, C. Zhang, C. Ren, J. Liu, Y. Zhang, J. Wang, F. Huang, L. Zhang, J. Liu, Supramolecular Hydrogel Based on Chlorambucil and Peptide Drug for Cancer Combination Therapy, ACS Appl. Mater. Interfaces. 11 (2019) 331–339. https://doi.org/10.1021/acsami.8b18425.

[66] Y. Gao, Y. Kuang, Z.-F. Guo, Z. Guo, I.J. Krauss, B. Xu, Enzyme-Instructed Molecular Self-assembly Confers Nanofibers and a Supramolecular Hydrogel of Taxol Derivative, J. Am. Chem. Soc. 131 (2009) 13576–13577. https://doi.org/10.1021/ja904411z.

[67] S. Barua, S. Mitragotri, Synergistic Targeting of Cell Membrane, Cytoplasm, and Nucleus of Cancer Cells Using Rod-Shaped Nanoparticles, ACS Nano. 7 (2013) 9558–9570. https://doi.org/10.1021/nn403913k.

[68] M. Ma, P. Xing, S. Xu, S. Li, X. Chu, A. Hao, Reversible pH-responsive helical nanoribbons formed using camptothecin, RSC Adv. 4 (2014) 42372–42375. https://doi.org/10.1039/C4RA08225G.

[69] Y. Wen, W. Zhang, N. Gong, Y.-F. Wang, H.-B. Guo, W. Guo, P.C. Wang, X.-J. Liang, Carrier-free, self-assembled pure drug nanorods composed of 10-hydroxycamptothecin and chlorin e6 for combinatorial chemo-photodynamic antitumor therapy in vivo, Nanoscale. 9 (2017) 14347–14356. https://doi.org/10.1039/C7NR03129G.

[70] Z. Zhou, Y. Piao, L. Hao, G. Wang, Z. Zhou, Y. Shen, Acidity-responsive shell-sheddable camptothecin-based nanofibers for carrier-free cancer drug delivery, Nanoscale. 11 (2019) 15907–15916. https://doi.org/10.1039/C9NR03872H.

[71] H. Kasai, T. Murakami, Y. Ikuta, Y. Koseki, K. Baba, H. Oikawa, H. Nakanishi, M. Okada, M. Shoji, M. Ueda, H. Imahori, M. Hashida, Creation of Pure Nanodrugs and Their Anticancer Properties, Angew. Chem. Int. Ed. 51 (2012) 10315–10318. https://doi.org/10.1002/anie.201204596.

[72] J. Kim, S. Michelin, M. Hilbers, L. Martinelli, E. Chaudan, G. Amselem, E. Fradet, J.-P. Boilot, A.M. Brouwer, C.N. Baroud, J. Peretti, T. Gacoin, Monitoring the orientation of rare-earth-doped nanorods for flow shear tomography, Nat. Nanotechnol. 12 (2017) 914–919. https://doi.org/10.1038/nnano.2017.111.

[73] V. Castelletto, P. Parras, I.W. Hamley, P. Bäverbäck, J.S. Pedersen, P. Panine, Wormlike Micelle Formation and Flow Alignment of a Pluronic Block Copolymer in Aqueous Solution, Langmuir. 23 (2007) 6896–6902. https://doi.org/10.1021/la700382y.

[74] V. Croce, T. Cosgrove, C.A. Dreiss, S. King, G. Maitland, T. Hughes, Giant Micellar Worms under Shear: A Rheological Study Using SANS, Langmuir. 21 (2005) 6762–6768. https://doi.org/10.1021/la0479410.

[75] P. Dalhaimer, F.S. Bates, D.E. Discher, Single Molecule Visualization of Stable, Stiffness-Tunable, Flow-Conforming Worm Micelles, Macromolecules. 36 (2003) 6873–6877. https://doi.org/10.1021/ma034120d.

[76] P.A. Stone, S.D. Hudson, P. Dalhaimer, D.E. Discher, E.J. Amis, K.B. Migler, Dynamics of Wormlike Micelles in Elongational Flows, Macromolecules. 39 (2006) 7144–7148. https://doi.org/10.1021/ma0611016.

[77] M. Müllner, S.J. Dodds, T.-H. Nguyen, D. Senyschyn, C.J.H. Porter, B.J. Boyd, F. Caruso, Size and Rigidity of Cylindrical Polymer Brushes Dictate Long Circulating Properties In Vivo, ACS Nano. 9 (2015) 1294–1304. https://doi.org/10.1021/nn505125f.

[78] E.J. Carboni, B.H. Bognet, G.M. Bouchillon, A.L. Kadilak, L.M. Shor, M.D. Ward, A.W.K. Ma, Direct Tracking of Particles and Quantification of Margination in Blood Flow, Biophys. J. 111 (2016) 1487–1495. https://doi.org/10.1016/j.bpj.2016.08.026.

[79] T.-R. Lee, M. Choi, A.M. Kopacz, S.-H. Yun, W.K. Liu, P. Decuzzi, On the near-wall accumulation of injectable particles in the microcirculation: smaller is not better, Sci. Rep. 3 (2013) 2079. https://doi.org/10.1038/srep02079.

[80] K. Müller, D.A. Fedosov, G. Gompper, Margination of micro- and nano-particles in blood flow and its effect on drug delivery, Sci. Rep. 4 (2015) 4871. https://doi.org/10.1038/srep04871.

[81] P. Kolhar, A.C. Anselmo, V. Gupta, K. Pant, B. Prabhakarpandian, E. Ruoslahti, S. Mitragotri, Using shape effects to target antibody-coated nanoparticles to lung and brain endothelium, Proc. Natl. Acad. Sci. 110 (2013) 10753–10758. https://doi.org/10.1073/pnas.1308345110.

[82] N. Doshi, B. Prabhakarpandian, A. Rea-Ramsey, K. Pant, S. Sundaram, S. Mitragotri, Flow and adhesion of drug carriers in blood vessels depend on their shape: A study using model synthetic microvascular networks, J. Controlled Release. 146 (2010) 196–200. https://doi.org/10.1016/j.jconrel.2010.04.007.

[83] M. Cooley, A. Sarode, M. Hoore, D.A. Fedosov, S. Mitragotri, A. Sen Gupta, Influence of particle size and shape on their margination and wall-adhesion: implications in drug delivery vehicle design across nano-to-micro scale, Nanoscale. 10 (2018) 15350–15364. https://doi.org/10.1039/C8NR04042G.

[84] K. Vahidkhah, P. Bagchi, Microparticle shape effects on margination, near-wall dynamics and adhesion in a three-dimensional simulation of red blood cell suspension, Soft Matter. 11 (2015) 2097–2109. https://doi.org/10.1039/C4SM02686A.

[85] S. Pawłowska, T.A. Kowalewski, F. Pierini, Fibrous polymer nanomaterials for biomedical applications and their transport by fluids: an overview, Soft Matter. 14 (2018) 8421–8444. https://doi.org/10.1039/C8SM01269E.

[86] V.V. Shuvaev, M.A. Ilies, E. Simone, S. Zaitsev, Y. Kim, S. Cai, A. Mahmud, T. Dziubla, S. Muro, D.E. Discher, V.R. Muzykantov, Endothelial Targeting of Antibody-Decorated Polymeric Filomicelles, ACS Nano. 5 (2011) 6991–6999. https://doi.org/10.1021/nn2015453.

[87] V.P. Chauhan, Z. Popović, O. Chen, J. Cui, D. Fukumura, M.G. Bawendi, R.K. Jain, Fluorescent Nanorods and Nanospheres for Real-Time In Vivo Probing of Nanoparticle Shape-Dependent Tumor Penetration, Angew. Chem. Int. Ed. 50 (2011) 11417–11420. https://doi.org/10.1002/anie.201104449.

[88] Y. Kim, P. Dalhaimer, D.A. Christian, D.E. Discher, Polymeric worm micelles as nano-carriers for drug delivery, Nanotechnology. 16 (2005) S484–S491. https://doi.org/10.1088/0957-4484/16/7/024.

[89] A. Pluen, P.A. Netti, R.K. Jain, D.A. Berk, Diffusion of Macromolecules in Agarose Gels: Comparison of Linear and Globular Configurations, Biophys. J. 77 (1999) 542–552. https://doi.org/10.1016/S0006-3495(99)76911-0.

[90] S. Shukla, F.J. Eber, A.S. Nagarajan, N.A. DiFranco, N. Schmidt, A.M. Wen, S. Eiben, R.M. Twyman, C. Wege, N.F. Steinmetz, The Impact of Aspect Ratio on the Biodistribution and Tumor Homing of Rigid Soft-Matter Nanorods, Adv. Healthc. Mater. 4 (2015) 874–882. https://doi.org/10.1002/adhm.201400641.

[91] H. Hillaireau, P. Couvreur, Nanocarriers' entry into the cell: relevance to drug delivery, Cell. Mol. Life Sci. 66 (2009) 2873–2896. https://doi.org/10.1007/s00018-009-0053-z.

[92] X. Banquy, F. Suarez, A. Argaw, J.-M. Rabanel, P. Grutter, J.-F. Bouchard, P. Hildgen, S. Giasson, Effect of mechanical properties of hydrogel nanoparticles on macrophage cell uptake, Soft Matter. 5 (2009) 3984. https://doi.org/10.1039/b821583a.

[93] X. Liu, F. Wu, Y. Tian, M. Wu, Q. Zhou, S. Jiang, Z. Niu, Size Dependent Cellular Uptake of Rod-like Bionanoparticles with Different Aspect Ratios, Sci. Rep. 6 (2016) 24567. https://doi.org/10.1038/srep24567.

[94] Y. Li, M. Kröger, W.K. Liu, Shape effect in cellular uptake of PEGylated nanoparticles: comparison between sphere, rod, cube and disk, Nanoscale. 7 (2015) 16631–16646. https://doi.org/10.1039/C5NR02970H.

[95] B.D. Chithrani, A.A. Ghazani, W.C.W. Chan, Determining the Size and Shape Dependence of Gold Nanoparticle Uptake into Mammalian Cells, Nano Lett. 6 (2006) 662–668. https://doi.org/10.1021/nl052396o.

[96] S. Barua, J.-W. Yoo, P. Kolhar, A. Wakankar, Y.R. Gokarn, S. Mitragotri, Particle shape enhances specificity of antibody-displaying nanoparticles, Proc. Natl. Acad. Sci. 110 (2013) 3270–3275. https://doi.org/10.1073/pnas.1216893110.

[97] M. Nowak, T.D. Brown, A. Graham, M.E. Helgeson, S. Mitragotri, Size, shape, and flexibility influence nanoparticle transport across brain endothelium under flow, Bioeng. Transl. Med. 5 (2020). https://doi.org/10.1002/btm2.10153.

[98] A. Banerjee, J. Qi, R. Gogoi, J. Wong, S. Mitragotri, Role of nanoparticle size, shape and surface chemistry in oral drug delivery, J. Controlled Release. 238 (2016) 176–185. https://doi.org/10.1016/j.jconrel.2016.07.051.

[99] D. Li, J. Zhuang, H. He, S. Jiang, A. Banerjee, Y. Lu, W. Wu, S. Mitragotri, L. Gan, J. Qi, Influence of Particle Geometry on Gastrointestinal Transit and Absorption following Oral Administration, ACS Appl. Mater. Interfaces. 9 (2017) 42492–42502. https://doi.org/10.1021/acsami.7b11821.

[100] S.E.A. Gratton, P.A. Ropp, P.D. Pohlhaus, J.C. Luft, V.J. Madden, M.E. Napier, J.M. DeSimone, The effect of particle design on cellular internalization pathways, Proc. Natl. Acad. Sci. 105 (2008) 11613–11618. https://doi.org/10.1073/pnas.0801763105.

[101] B. Karagoz, L. Esser, H.T. Duong, J.S. Basuki, C. Boyer, T.P. Davis, Polymerization-Induced Self-Assembly (PISA) – control over the morphology of nanoparticles for drug delivery applications, Polym Chem. 5 (2014) 350–355. https://doi.org/10.1039/C3PY01306E.

[102] Z. Zhou, X. Ma, E. Jin, J. Tang, M. Sui, Y. Shen, E.A. Van Kirk, W.J. Murdoch, M. Radosz, Linear-dendritic drug conjugates forming long-circulating nanorods for cancer-drug delivery, Biomaterials. 34 (2013) 5722–5735. https://doi.org/10.1016/j.biomaterials.2013.04.012.

[103] A. Schulz, S. Jaksch, R. Schubel, E. Wegener, Z. Di, Y. Han, A. Meister, J. Kressler, A.V. Kabanov, R. Luxenhofer, C.M. Papadakis, R. Jordan, Drug-Induced Morphology Switch in Drug Delivery Systems Based on Poly(2-oxazoline)s, ACS Nano. 8 (2014) 2686–2696. https://doi.org/10.1021/nn406388t.

[104] S.M. Loverde, M.L. Klein, D.E. Discher, Nanoparticle Shape Improves Delivery: Rational Coarse Grain Molecular Dynamics (rCG-MD) of Taxol in Worm-Like PEG-PCL Micelles, Adv. Mater. 24 (2012) 3823–3830. https://doi.org/10.1002/adma.201103192.

[105] W. Li, X. Zhang, X. Hao, J. Jie, B. Tian, X. Zhang, Shape design of high drug payload nanoparticles for more effective cancer therapy, Chem. Commun. 49 (2013) 10989. https://doi.org/10.1039/c3cc46718j.

[106] M. Zhou, X. Zhang, C. Yu, X. Nan, X. Chen, X. Zhang, Shape regulated anticancer activities and systematic toxicities of drug nanocrystals in vivo, Nanomedicine Nanotechnol. Biol. Med. 12 (2016) 181–189. https://doi.org/10.1016/j.nano.2015.09.006.

[107] Y. Li, J. Lin, Y. Huang, Y. Li, X. Yang, H. Wu, S. Wu, L. Xie, L. Dai, Z. Hou, Self-Targeted, Shape-Assisted, and Controlled-Release Self-Delivery Nanodrug for Synergistic Targeting/Anticancer Effect of Cytoplasm and Nucleus of Cancer Cells, ACS Appl. Mater. Interfaces. 7 (2015) 25553–25559. https://doi.org/10.1021/acsami.5b07348.

[108] E. Lepeltier, C. Bourgaux, A. Maksimenko, F. Meneau, V. Rosilio, E. Sliwinski, F. Zouhiri, D. Desmaële, P. Couvreur, Self-Assembly of Polyisoprenoyl Gemcitabine Conjugates: Influence of Supramolecular Organization on Their Biological Activity, Langmuir. 30 (2014) 6348–6357. https://doi.org/10.1021/la5007132.

[109] Y. Mai, A. Eisenberg, Self-assembly of block copolymers, Chem. Soc. Rev. 41 (2012) 5969. https://doi.org/10.1039/c2cs35115c.

[110] Y.-Y. Won, H.T. Davis, F.S. Bates, Giant Wormlike Rubber Micelles, Science. 283 (1999) 960–963. https://doi.org/10.1126/science.283.5404.960.

[111] Y.-Y. Won, A.K. Brannan, H.T. Davis, F.S. Bates, Cryogenic Transmission Electron Microscopy (Cryo-TEM) of Micelles and Vesicles Formed in Water by Poly(ethylene oxide)-

Based Block Copolymers, J. Phys. Chem. B. 106 (2002) 3354–3364. https://doi.org/10.1021/jp013639d.

[112] S. Jain, On the Origins of Morphological Complexity in Block Copolymer Surfactants, Science. 300 (2003) 460–464. https://doi.org/10.1126/science.1082193.

[113] K. Rajagopal, A. Mahmud, D.A. Christian, J.D. Pajerowski, A.E.X. Brown, S.M. Loverde, D.E. Discher, Curvature-Coupled Hydration of Semicrystalline Polymer Amphiphiles Yields flexible Worm Micelles but Favors Rigid Vesicles: Polycaprolactone-Based Block Copolymers, Macromolecules. 43 (2010) 9736–9746. https://doi.org/10.1021/ma101316w.

[114] N. Petzetakis, A.P. Dove, R.K. O'Reilly, Cylindrical micelles from the living crystallization-driven self-assembly of poly(lactide)-containing block copolymers, Chem Sci. 2 (2011) 955–960. https://doi.org/10.1039/C0SC00596G.

[115] G. Rizis, T.G.M. van de Ven, A. Eisenberg, Crystallinity-driven morphological ripening processes for poly(ethylene oxide)-block-polycaprolactone micelles in water, Soft Matter. 10 (2014) 2825. https://doi.org/10.1039/c3sm52950a.

[116] J. Zhang, L.-Q. Wang, H. Wang, K. Tu, Micellization Phenomena of Amphiphilic Block Copolymers Based on Methoxy Poly(ethylene glycol) and Either Crystalline or Amorphous Poly(caprolactone- b -lactide), Biomacromolecules. 7 (2006) 2492–2500. https://doi.org/10.1021/bm0601732.

[117] J.C. Foster, S. Varlas, B. Couturaud, Z. Coe, R.K. O'Reilly, Getting into Shape: Reflections on a New Generation of Cylindrical Nanostructures' Self-Assembly Using Polymer Building Blocks, J. Am. Chem. Soc. 141 (2019) 2742–2753. https://doi.org/10.1021/jacs.8b08648.

[118] C. Hörtz, A. Birke, L. Kaps, S. Decker, E. Wächtersbach, K. Fischer, D. Schuppan, M. Barz, M. Schmidt, Cylindrical Brush Polymers with Polysarcosine Side Chains: A Novel Biocompatible Carrier for Biomedical Applications, Macromolecules. 48 (2015) 2074–2086. https://doi.org/10.1021/ma502497x.

[119] Y. Geng, D.E. Discher, Visualization of degradable worm micelle breakdown in relation to drug release, Polymer. 47 (2006) 2519–2525. https://doi.org/10.1016/j.polymer.2005.11.093.

[120] N.S. Oltra, J. Swift, A. Mahmud, K. Rajagopal, S.M. Loverde, D.E. Discher, Filomicelles in nanomedicine – from flexible, fragmentable, and ligand-targetable drug carrier designs to combination therapy for brain tumors, J. Mater. Chem. B. 1 (2013) 5177. https://doi.org/10.1039/c3tb20431f.

[121] P.R. Nair, C. Alvey, X. Jin, J. Irianto, I. Ivanovska, D.E. Discher, Filomicelles Deliver a Chemo-Differentiation Combination of Paclitaxel and Retinoic Acid That Durably Represses Carcinomas in Liver to Prolong Survival, Bioconjug. Chem. (2018). https://doi.org/10.1021/acs.bioconjchem.7b00816.

[122] Y. Geng, D.E. Discher, Hydrolytic Degradation of Poly(ethylene oxide)- block-Polycaprolactone Worm Micelles, J. Am. Chem. Soc. 127 (2005) 12780–12781. https://doi.org/10.1021/ja053902e.

[123] H. Yu, Z. Xu, D. Wang, X. Chen, Z. Zhang, Q. Yin, Y. Li, Intracellular pH-activated PEG-b-PDPA wormlike micelles for hydrophobic drug delivery, Polym. Chem. 4 (2013) 5052. https://doi.org/10.1039/c3py00849e.

[124] J.O. Lee, K.T. Oh, D. Kim, E.S. Lee, pH-sensitive short worm-like micelles targeting tumors based on the extracellular pH, J Mater Chem B. 2 (2014) 6363–6370. https://doi.org/10.1039/C4TB00779D.

[125] N. Parker, M.J. Turk, E. Westrick, J.D. Lewis, P.S. Low, C.P. Leamon, Folate receptor expression in carcinomas and normal tissues determined by a quantitative radioligand binding assay, Anal. Biochem. 338 (2005) 284–293. https://doi.org/10.1016/j.ab.2004.12.026.

[126] A. Trent, R. Marullo, B. Lin, M. Black, M. Tirrell, Structural properties of soluble peptide amphiphile micelles, Soft Matter. 7 (2011) 9572. https://doi.org/10.1039/c1sm05862b.

[127] S.E. Paramonov, H.-W. Jun, J.D. Hartgerink, Self-Assembly of Peptide−Amphiphile Nanofibers: The Roles of Hydrogen Bonding and Amphiphilic Packing, J. Am. Chem. Soc. 128 (2006) 7291–7298. https://doi.org/10.1021/ja060573x.

[128] T. Shimada, S. Lee, F.S. Bates, A. Hotta, M. Tirrell, Wormlike Micelle Formation in Peptide-Lipid Conjugates Driven by Secondary Structure Transformation of the Headgroups †, J. Phys. Chem. B. 113 (2009) 13711–13714. https://doi.org/10.1021/jp901727q.

[129] T. Shimada, N. Sakamoto, R. Motokawa, S. Koizumi, M. Tirrell, Self-Assembly Process of Peptide Amphiphile Worm-Like Micelles, J. Phys. Chem. B. 116 (2012) 240–243. https://doi.org/10.1021/jp209105z.

[130] M.J. Webber, E.J. Berns, S.I. Stupp, Supramolecular Nanofibers of Peptide Amphiphiles for Medicine, Isr. J. Chem. 53 (2013) 530–554. https://doi.org/10.1002/ijch.201300046.

[131] K. Temming, R.M. Schiffelers, G. Molema, R.J. Kok, RGD-based strategies for selective delivery of therapeutics and imaging agents to the tumour vasculature, Drug Resist. Updat. 8 (2005) 381–402. https://doi.org/10.1016/j.drup.2005.10.002.

[132] G. Cinar, A. Ozdemir, S. Hamsici, G. Gunay, A. Dana, A.B. Tekinay, M.O. Guler, Local delivery of doxorubicin through supramolecular peptide amphiphile nanofiber gels, Biomater. Sci. 5 (2017) 67–76. https://doi.org/10.1039/C6BM00656F.

[133] C. Luo, J. Sun, B. Sun, Z. He, Prodrug-based nanoparticulate drug delivery strategies for cancer therapy, Trends Pharmacol. Sci. 35 (2014) 556–566. https://doi.org/10.1016/j.tips.2014.09.008.

[134] W. Ma, A.G. Cheetham, H. Cui, Building nanostructures with drugs, Nano Today. 11 (2016) 13–30. https://doi.org/10.1016/j.nantod.2015.11.003.

[135] F. Baldelli Bombelli, D. Berti, U. Keiderling, P. Baglioni, Giant Polymerlike Micelles Formed by Nucleoside-Functionalized Lipids, J. Phys. Chem. B. 106 (2002) 11613–11621. https://doi.org/10.1021/jp020463m.

[136] A. Maksimenko, F. Dosio, J. Mougin, A. Ferrero, S. Wack, L.H. Reddy, A.-A. Weyn, E. Lepeltier, C. Bourgaux, B. Stella, L. Cattel, P. Couvreur, A Unique Squalenoylated and Nonpegylated Doxorubicin Nanomedicine with Systemic Long-Circulating Properties and Anticancer Activity, Proc. Natl. Acad. Sci. 111 (2014) E217–E226. https://doi.org/10.1073/pnas.1313459110.

[137] H. Su, P. Zhang, A.G. Cheetham, J.M. Koo, R. Lin, A. Masood, P. Schiapparelli, A. Quiñones-Hinojosa, H. Cui, Supramolecular Crafting of Self-Assembling Camptothecin Prodrugs with Enhanced Efficacy against Primary Cancer Cells, Theranostics. 6 (2016) 1065–1074. https://doi.org/10.7150/thno.15420.

[138] Y. Zhou, L. Lei, Z. Zhang, R. Zhang, Q. Song, X. Li, Cation instructed steroidal prodrug supramolecular hydrogel, J. Colloid Interface Sci. 528 (2018) 10–17. https://doi.org/10.1016/j.jcis.2018.05.059.

[139] T. Xiong, X. Li, Y. Zhou, Q. Song, R. Zhang, L. Lei, X. Li, Glycosylation-enhanced biocompatibility of the supramolecular hydrogel of an anti-inflammatory drug for topical suppression of inflammation, Acta Biomater. 73 (2018) 275–284. https://doi.org/10.1016/j.actbio.2018.04.019.

[140] N.P. Truong, J.F. Quinn, M.R. Whittaker, T.P. Davis, Polymeric filomicelles and nanoworms: two decades of synthesis and application, Polym Chem. 7 (2016) 4295–4312. https://doi.org/10.1039/C6PY00639F.

[141] D. Berti, C. Montis, P. Baglioni, Self-assembly of designer biosurfactants, Soft Matter. 7 (2011) 7150–7158. https://doi.org/10.1039/c1sm05197k.

[142] A. Gissot, M. Camplo, M.W. Grinstaff, P. Barthélémy, Nucleoside, nucleotide and oligonucleotide based amphiphiles: a successful marriage of nucleic acids with lipids, Org. Biomol. Chem. 6 (2008) 1324. https://doi.org/10.1039/b719280k.

[143] J. Baillet, V. Desvergnes, A. Hamoud, L. Latxague, P. Barthélémy, Lipid and Nucleic Acid Chemistries: Combining the Best of Both Worlds to Construct Advanced Biomaterials, Adv. Mater. 30 (2018) 1705078. https://doi.org/10.1002/adma.201705078.

[144] P. Sandin, F.B. Bombelli, B. Castroflorio, C. Müller, J. Obermeier, G. Karlsson, K. Edwards, P. Baglioni, D. Berti, Diastereoselective self-assembly of clofarabine lipids, New J Chem. 38 (2014) 5247–5253. https://doi.org/10.1039/C4NJ00856A.

[145] P. Couvreur, B. Stella, L.H. Reddy, H. Hillaireau, C. Dubernet, D. Desmaële, S. Lepêtre-Mouelhi, F. Rocco, N. Dereuddre-Bosquet, P. Clayette, V. Rosilio, V. Marsaud, J.-M. Renoir, L. Cattel, Squalenoyl Nanomedicines as Potential Therapeutics, Nano Lett. 6 (2006) 2544–2548. https://doi.org/10.1021/nl061942q.

[146] L. Kotelevets, E. Chastre, J. Caron, J. Mougin, G. Bastian, A. Pineau, F. Walker, T. Lehy, D. Desmaële, P. Couvreur, A Squalene-Based Nanomedicine for Oral Treatment of Colon Cancer, Cancer Res. 77 (2017) 2964–2975. https://doi.org/10.1158/0008-5472.CAN-16-1741.

[147] D. Sobot, S. Mura, S.O. Yesylevskyy, L. Dalbin, F. Cayre, G. Bort, J. Mougin, D. Desmaële, S. Lepetre-Mouelhi, G. Pieters, B. Andreiuk, A.S. Klymchenko, J.-L. Paul, C. Ramseyer, P. Couvreur, Conjugation of squalene to gemcitabine as unique approach exploiting endogenous lipoproteins for drug delivery, Nat. Commun. 8 (2017) 15678. https://doi.org/10.1038/ncomms15678.

[148] A. Gaudin, M. Yemisci, H. Eroglu, S. Lepetre-Mouelhi, O.F. Turkoglu, B. Dönmez-Demir, S. Caban, M.F. Sargon, S. Garcia-Argote, G. Pieters, O. Loreau, B. Rousseau, O. Tagit, N. Hildebrandt, Y. Le Dantec, J. Mougin, S. Valetti, H. Chacun, V. Nicolas, D. Desmaële, K. Andrieux, Y. Capan, T. Dalkara, P. Couvreur, Squalenoyl Adenosine Nanoparticles Provide Neuroprotection After Stroke and Spinal Cord Injury, Nat. Nanotechnol. 9 (2014) 1054–1062. https://doi.org/10.1038/nnano.2014.274.

[149] J. Feng, S. Lepetre-Mouelhi, A. Gautier, S. Mura, C. Cailleau, F. Coudore, M. Hamon, P. Couvreur, A new painkiller nanomedicine to bypass the blood-brain barrier and the use of morphine, Sci. Adv. 5 (2019) eaau5148. https://doi.org/10.1126/sciadv.aau5148.

[150] F. Dormont, R. Brusini, C. Cailleau, F. Reynaud, A. Peramo, A. Gendron, J. Mougin, F. Gaudin, M. Varna, P. Couvreur, Squalene-based multidrug nanoparticles for improved mitigation of uncontrolled inflammation, Sci. Adv. (2020) eaaz5466. https://doi.org/10.1126/sciadv.aaz5466.

[151] Y. Wang, A.G. Cheetham, G. Angacian, H. Su, L. Xie, H. Cui, Peptide–drug conjugates as effective prodrug strategies for targeted delivery, Adv. Drug Deliv. Rev. 110–111 (2017) 112–126. https://doi.org/10.1016/j.addr.2016.06.015.

[152] M. Kang, P. Zhang, H. Cui, S.M. Loverde, π–π Stacking Mediated Chirality in Functional Supramolecular Filaments, Macromolecules. 49 (2016) 994–1001. https://doi.org/10.1021/acs.macromol.5b02148.

[153] A.G. Cheetham, Y.-C. Ou, P. Zhang, H. Cui, Linker-determined drug release mechanism of free camptothecin from self-assembling drug amphiphiles, Chem Commun. 50 (2014) 6039–6042. https://doi.org/10.1039/C3CC49453E.

[154] M.J. Webber, J.B. Matson, V.K. Tamboli, S.I. Stupp, Controlled release of dexamethasone from peptide nanofiber gels to modulate inflammatory response, Biomaterials. 33 (2012) 6823–6832. https://doi.org/10.1016/j.biomaterials.2012.06.003.

[155] S. Das, H. Horo, U. Goswami, L.M. Kundu, Synthesis of a Peptide Conjugated 5-Fluorouracil Gelator Prodrug for Photo-Controlled Release of the Antitumor Agent, ChemistrySelect. 4 (2019) 6778–6783. https://doi.org/10.1002/slct.201900905.

[156] J. Li, Y. Gao, Y. Kuang, J. Shi, X. Du, J. Zhou, H. Wang, Z. Yang, B. Xu, Dephosphorylation of D-Peptide Derivatives to Form Biofunctional, Supramolecular Nanofibers/Hydrogels and Their Potential Applications for Intracellular Imaging and Intratumoral Chemotherapy, J. Am. Chem. Soc. 135 (2013) 9907–9914. https://doi.org/10.1021/ja404215g.

[157] R.W. Chakroun, F. Wang, R. Lin, Y. Wang, H. Su, D. Pompa, H. Cui, Fine-Tuning the Linear Release Rate of Paclitaxel-Bearing Supramolecular Filament Hydrogels through Molecular Engineering, ACS Nano. (2019). https://doi.org/10.1021/acsnano.9b01689.

[158] W.A. Henne, D.D. Doorneweerd, A.R. Hilgenbrink, S.A. Kularatne, P.S. Low, Synthesis and activity of a folate peptide camptothecin prodrug, Bioorg. Med. Chem. Lett. 16 (2006) 5350–5355. https://doi.org/10.1016/j.bmcl.2006.07.076.

[159] S.-Y. Qin, Y.-J. Cheng, Z.-W. Jiang, Y.-H. Ma, A.-Q. Zhang, Morphology control of self-deliverable nanodrug with enhanced anticancer efficiency, Colloids Surf. B Biointerfaces. 165 (2018) 345–354. https://doi.org/10.1016/j.colsurfb.2018.02.054.

[160] S.-Y. Qin, M.-Y. Peng, L. Rong, B. Li, S.-B. Wang, S.-X. Cheng, R.-X. Zhuo, X.-Z. Zhang, Self-defensive nano-assemblies from camptothecin-based antitumor drugs, Regen. Biomater. 2 (2015) 159–166. https://doi.org/10.1093/rb/rbv011.

[161] V. Bala, S. Rao, B.J. Boyd, C.A. Prestidge, Prodrug and nanomedicine approaches for the delivery of the camptothecin analogue SN38, J. Controlled Release. 172 (2013) 48–61. https://doi.org/10.1016/j.jconrel.2013.07.022.

[162] H. Zhao, C. Lee, P. Sai, Y.H. Choe, M. Boro, A. Pendri, S. Guan, R.B. Greenwald, 20- O -Acylcamptothecin Derivatives: Evidence for Lactone Stabilization, J. Org. Chem. 65 (2000) 4601–4606. https://doi.org/10.1021/jo000221n.

[163] H.-G. Lerchen, J. Baumgarten, K. von dem Bruch, T.E. Lehmann, M. Sperzel, G. Kempka, H.-H. Fiebig, Design and Optimization of 20-O-Linked Camptothecin Glycoconjugates as Anticancer Agents, J. Med. Chem. 44 (2001) 4186–4195. https://doi.org/10.1021/jm010893l.

[164] Y. Li, X. Hu, X. Zheng, Y. Liu, S. Liu, Y. Yue, Z. Xie, Self-assembled organic nanorods for dual chemo-photodynamic therapies, RSC Adv. 8 (2018) 5493–5499. https://doi.org/10.1039/C8RA00067K.

[165] Y. Guo, T. Wang, H. Qiu, M. Han, Z. Dong, X. Wang, Y. Wang, Hydroxycamptothecin nanoparticles based on poly/oligo (ethylene glycol): Architecture effects of nanocarriers on antitumor efficacy, Eur. J. Pharm. Biopharm. 134 (2019) 178–184. https://doi.org/10.1016/j.ejpb.2018.12.003.

[166] H. Li, Y. Li, H. Ao, J. Fu, Y. Guo, M. Han, X. Yan, X. Chen, X. Wang, A comparative study on the in vitro and in vivo antitumor efficacy of icaritin and hydrous icaritin nanorods, Drug Deliv. 27 (2020) 1176–1187. https://doi.org/10.1080/10717544.2020.1801892.

[167] C. Kinnear, T.L. Moore, L. Rodriguez-Lorenzo, B. Rothen-Rutishauser, A. Petri-Fink, Form Follows Function: Nanoparticle Shape and Its Implications for Nanomedicine, Chem. Rev. 117 (2017) 11476–11521. https://doi.org/10.1021/acs.chemrev.7b00194.

[168] C.A. Poland, R. Duffin, I. Kinloch, A. Maynard, W.A.H. Wallace, A. Seaton, V. Stone, S. Brown, W. MacNee, K. Donaldson, Carbon nanotubes introduced into the abdominal cavity of mice show asbestos-like pathogenicity in a pilot study, Nat. Nanotechnol. 3 (2008) 423–428. https://doi.org/10.1038/nnano.2008.111.

[169] M.L. Schipper, N. Nakayama-Ratchford, C.R. Davis, N.W.S. Kam, P. Chu, Z. Liu, X. Sun, H. Dai, S.S. Gambhir, A pilot toxicology study of single-walled carbon nanotubes in a small sample of mice, Nat. Nanotechnol. 3 (2008) 216–221. https://doi.org/10.1038/nnano.2008.68.

[170] R. Liu, Y. Jiang, X. Hu, J. Wu, W. Jiang, G. Jin, Y. Luan, A preclinical evaluation of cytarabine prodrug nanofibers assembled from cytarabine-lauric acid conjugate toward solid tumors, Int. J. Pharm. 552 (2018) 111–118. https://doi.org/10.1016/j.ijpharm.2018.09.043.

[171] N.A. Mansukhani, E.B. Peters, M.M. So, M.S. Albaghdadi, Z. Wang, M.R. Karver, T.D. Clemons, J.P. Laux, N.D. Tsihlis, S.I. Stupp, M.R. Kibbe, Peptide Amphiphile Supramolecular

Nanostructures as a Targeted Therapy for Atherosclerosis, Macromol. Biosci. 19 (2019) 1900066. https://doi.org/10.1002/mabi.201900066.